



The Miocene lacustrine carbonate factory of the Ñirihuau Formation, Ñirihuau Basin, North Patagonian Andes, Argentina

Camila Santonja¹  | Cecilia A. Benavente^{2,3}  | Julieta Suriano² |
 Arturo M. Heredia⁴ | Natalia Fortunatti⁵ | Ana L. Rainoldi^{5,6} |
 Diego A. Kietzmann¹ | Florencia Bechis⁷

¹Instituto de Geociencias Básicas, Aplicadas y Ambientales de Buenos Aires (IGEBA), Universidad de Buenos Aires-CONICET, Ciudad Universitaria, Pabellón II, Intendente Güiraldes 2160 (C1428EHA), Buenos Aires, Argentina

²Instituto Argentino de Nivología, Glaciología y Ciencias Ambientales (IANIGLA), CCT Mendoza, CONICET, Mendoza, Argentina

³Geología, Facultad de Ciencias Exactas y Naturales, Universidad Nacional de Cuyo, Mendoza, Argentina

⁴Instituto de Investigación en Paleobiología y Geología (IIPG), Universidad Nacional de Río Negro-CONICET, General Roca, Argentina

⁵Departamento de Geología, Universidad Nacional del Sur, Bahía Blanca, Argentina

⁶Instituto Geológico del Sur (INGEOSUR), Universidad Nacional del Sur-CONICET, Bahía Blanca, Argentina

⁷Instituto de Investigaciones en Diversidad Cultural y Procesos de Cambio (IIDyPCa), Universidad Nacional de Río Negro-CONICET, San Carlos de Bariloche, Argentina

Correspondence

Camila Santonja, Instituto de Geociencias Básicas, Aplicadas y Ambientales de Buenos Aires (IGEBA), Universidad de Buenos Aires-CONICET, Ciudad Universitaria, Pabellón II, Intendente Güiraldes 2160 (C1428EHA), Buenos Aires, Argentina.
 Email: cs.santonja@gmail.com

Cecilia A. Benavente, Instituto Argentino de Nivología, Glaciología y Ciencias Ambientales (IANIGLA), CCT Mendoza, CONICET, Mendoza, Argentina.
 Email: ceciliabenavente@fcen.uncu.edu.ar

Funding information

Agencia Nacional de Promoción Científica y Tecnológica, Grant/Award Number: PICT 2020-2619, PICT-2017-3259 and PICT-2018-2356; Universidad Nacional de Río Negro, Grant/Award Number: 40-B-743; CONICET, Grant/Award Number: PIP-2021-0818

Abstract

Facies, microfacies and stable isotope analyses of limestone beds in the northernmost Ñirihuau Basin, North Patagonian Andes, Argentina, document and constrain the past hydrological, sedimentological and climate conditions that prevailed during the deposition of a lacustrine system between *ca* 15 and 13 Ma. This palaeoenvironment is recorded in the middle section of the Ñirihuau Formation, which holds significance because: (1) It was deposited during a transition from an extensional to a compressional tectonic regime; (2) it spans the Middle Miocene Climatic Optimum and the beginning of the Middle Miocene Climatic Transition; and (3) it contains limestone beds interbedded within a 600 m thick interval of mudstones and siltstones, along with intercalated sandstone and volcanoclastic bodies. Two detailed sedimentary logs were surveyed along the Arroyo Las Bayas, at the western and eastern flank of the David Syncline. Limestones from both stratigraphic sections were sampled as well as isolated limestone beds from two other sites. One facies association was defined and interpreted as a perennial lake associated with a deltaic system and dominated by detrital clastic material. It comprises Facies 1 (Marginal lacustrine) and Facies 2 (Lower delta plain); in both, the presence of grainstones and calcimudstones stands out. Through petrography and cathodoluminescence studies of these

This is an open access article under the terms of the [Creative Commons Attribution](https://creativecommons.org/licenses/by/4.0/) License, which permits use, distribution and reproduction in any medium, provided the original work is properly cited.

© 2024 The Author(s). *The Depositional Record* published by John Wiley & Sons Ltd on behalf of International Association of Sedimentologists.

continental carbonates, nine microfacies were identified: (a) Intraclastic grainstone, (b) Homogeneous calcimudstone, (c) Silty grainstone, (d) Disrupted micrite, (e) Birds eye micrite, (f) Bioclastic mudstone, (g) Calcimudstone with sparse detrital grains, (h) Fenestral micrite, (i) Stromatolitic boundstone. These indicate mainly bio-induced subaqueous carbonate precipitation and subordinate deposition by tractive flows with short-distance transport on a littoral lacustrine environment. Most of these microfacies exhibit very early diagenesis (eogenesis) effects. These features, and the geochemistry results, indicate that they were deposited in a palaeolake system under temperate to warm and humid conditions.

KEYWORDS

carbonates, cathodoluminescence, Miocene, Patagonia, petrography $\delta^{13}\text{C}$ and $\delta^{18}\text{O}$ stable isotopes

1 | INTRODUCTION

Understanding hydrology in deep time is critical when reconstructing the evolution of palaeolake systems and for recognising the factors that influenced their sedimentation and ecosystems (Talbot, 1990; Gierlowski-Kordesch & Kelts, 1994; Carroll & Bohacs, 1999; Bohacs & Suter, 1997; Bohacs et al., 2000, 2003). Climate and tectonics are the primary and co-equal influencing factors on hydrology, palaeogeography (basin configuration) and sediment supply, making isolating the main drivers of palaeo-hydrological regimes challenging (Vázquez-Urbez et al., 2013; Benavente et al., 2021). In addition, availability and quality of outcrops can make it difficult to discern the spatial pattern of hydrology and sedimentation in lake systems.

Stratigraphic data, combined with geochemical, petrographic and sedimentological analyses of continental carbonates, can provide valuable insights into the hydrological regimes of ancient lake basins (Talbot, 1990; Valero-Garcés et al., 1997; Arenas et al., 1997; Arenas & Pardo, 1999; Swart, 2015). The analysis of stable isotope ratios ($\delta^{13}\text{C}$ and $\delta^{18}\text{O}$) in primary carbonate lacustrine sediments is a valuable tool in palaeolimnology and limnogeology, because it provides insights into the chemical composition of palaeolake waters and the palaeohydrological variations at the basin scale (Kelts & Talbot, 1990; Talbot, 1990; Camoin et al., 1997; Ricketts & Anderson, 1998; Leng et al., 2005; Vázquez-Urbez et al., 2013; Christ et al., 2018). Nevertheless, such studies demand careful sampling and examination to distinguish primary sediments from secondary features that record processes that could have altered the primary isotopic signature (Murphy et al., 2014; Swart, 2015). Interpretation of stable isotopic data in their sedimentological and palaeogeographical context allows the

accurate identification of primary features that record palaeoclimate (Kelts & Talbot, 1990; Leng et al., 2005), the chemical composition of the lake waters and potential effects of biological activity during carbonate precipitation (Guo et al., 1996; Andres et al., 2006).

In this sense, the Ñirihuau Formation of the Ñirihuau Basin (Figure 1), located on the eastern slope of the North Patagonian Andes of Argentina, is an ideal case for this kind of study, because it records the palaeoenvironmental and tectonic evolution of this region during the Miocene (Cazau, 1972, 1980; Cazau et al., 1989, 2005; Mancini & Serna, 1989; Bechis, 2004; Bechis & Cristallini, 2006; Paredes et al., 2009; Bechis et al., 2014b; Orts et al., 2015; Ramos et al., 2015; Butler et al., 2020; Santonja et al., 2021). Moreover, the middle section of this unit contains thick lacustrine deposits with limestone beds that allow microfacies and carbon and oxygen stable isotope studies because they offer a well-preserved record of sedimentary processes, and can provide valuable insights into past hydrodynamics, depositional dynamics and climate conditions.

The lacustrine middle section of the Ñirihuau Formation was deposited between *ca* 15 and 13 Ma (Langhian–Serravallian) according to available U–Pb geochronology (Santonja et al., 2021). Its deposition was coincident with the Middle Miocene Climatic Optimum (MMCO), which is a warm wet phase that began in the Early Miocene with elevated global temperatures that peaked from 17 to 15 Ma (Zachos et al., 2001), and the Middle Miocene Climatic Transition (MMCT, *ca* 14.5–13 Ma), that marked the beginning of a global cooling (Leutert et al., 2021). Climate conditions during the Miocene have been broadly studied in Chile and Argentina, both in the Andean and extra-Andean regions, by analysing the relationship between climate and vegetation, fauna or the sedimentary record (MacFadden et al., 1996; Hinojosa, 2005; Hinojosa

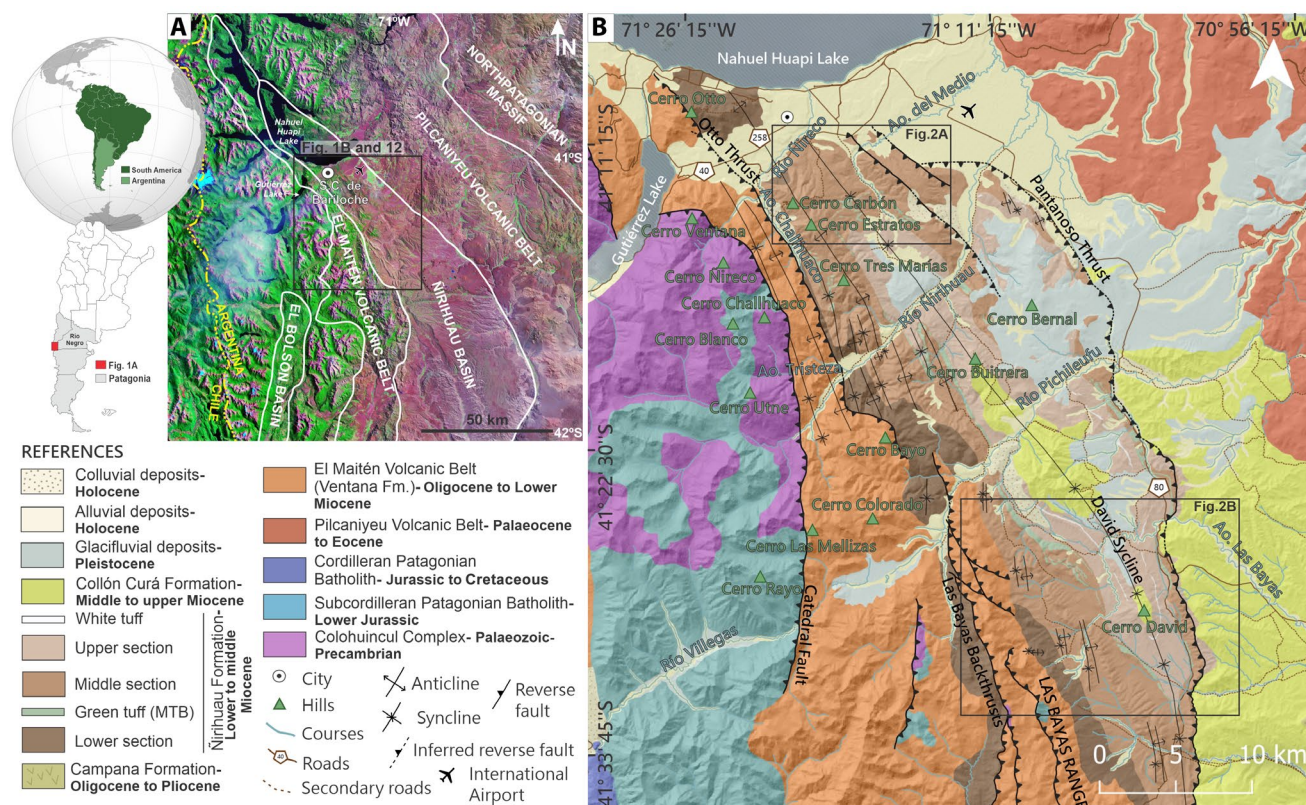


FIGURE 1 Location map of the Ñirihuau Basin. (A) Landsat™ mosaic-based map showing the main regional morpho-structural units (modified from Bechis et al., 2014b). (B) Regional geologic map of the Ñirihuau Basin showing the geologic units and the main structures of the study area (after González Bonorino, 1944; González et al., 2000; Giacosa et al., 2001; SERNAGEOMIN, 2003; Bechis et al., 2014b; Santonja et al., 2021). MTB: 'Miembro Tobas y Brechas' defined by González Bonorino and González Bonorino (1978).

& Gutiérrez, 2009; Kohn et al., 2015; Carrapa et al., 2019; Raigemborn et al., 2021; Aramendía et al., 2023; Bilmes et al., 2014; Bucher et al., 2020, 2021, among others). However, few studies have been carried out on carbonate beds from lacustrine basins of the Andean region of southern South America (Alonso-Zarza et al., 2020).

The lacustrine facies of the middle section of the Ñirihuau Formation (Santonja et al., 2021) constitute a thick vertical interval (up to 600 m) of tabular mudstone beds with intercalations of tabular to lentiform sandstone beds, volcanoclastic deposits such as tuffs and lapilli-tuffs and limestones. It has been interpreted as a perennial lake dominated by detrital clastic material that contains shallowing-upward successions and syndepositional volcanism (ash-fall and pyroclastic flow deposits; Paredes et al., 2009; Santonja et al., 2021). However, there have been no studies on the hydrological conditions of this lacustrine system, and the relationship between the sedimentation patterns and the lake-basin type remains unexplored.

This contribution provides new and detailed sedimentological, petrographic and geochemical information for two stratigraphic sections of the lacustrine facies

from the middle section of the Ñirihuau Formation along the Arroyo Las Bayas (Figure 1B). These sections are situated on both flanks of the David Syncline and are laterally in a similar interval of the unit (Arroyo Las Bayas and Cerro David sites). They were chosen due to the quality of the outcrops that contain limestone intercalations. Petrographic and geochemical analyses were also performed on samples of limestone beds from the Ñirihuau Formation of two other sites (Cerro Carbón and Arroyo del Medio, Figure 1B), located towards the north of the basin.

The main purpose of this research is to characterise the carbonate factory of the basin, which will allow a better understanding of the hydrological and palaeoclimate conditions that prevailed during its deposition. The analysis of these strata could provide the key to classifying the lake basin as either an overfilled or balanced-fill type. Moreover, the new data allow us to evaluate a possible link with the global climate at that time. This study holds significance as it represents one of the first contributions about continental carbonate records for the Miocene of southern South America that addresses their implications for the climate of Patagonia during the MMCO. Therefore,

the results herein provide a unique perspective about the conditions during deposition of the lacustrine facies of the Ñirihuau Formation between 15 and 13 Ma.

2 | GEOLOGICAL SETTING

An important plate reorganisation took place during the Oligocene to Miocene, when the Farallón Plate split into the Nazca and Cocos plates, and the convergence between the South American and Nazca plates experienced a sudden acceleration and a shift towards an almost orthogonal direction (Pardo-Casas & Molnar, 1987; Somoza, 1998). During this time, several basins developed in the Andes region between 33° and 45°S filled with thick successions of volcanic and sedimentary rocks, deposited in continental or marine environments (Jordan et al., 2001). Two main basins have been identified near the study area: Ñirihuau and El Bolsón (Figure 1A). It has been proposed that they could have been originally linked but were later disconnected due to uplift of basement blocks during the main Andean contractional deformation in the Neogene (Figure 1A; Ramos, 1982; Spalletti, 1983; Giacosa & Heredia, 1999, 2004; Cazau et al., 2005; Paredes et al., 2009; Asensio et al., 2010). The western depocentres correspond to the El Bolsón Basin, which includes Oligocene to Miocene marine and continental sequences from the El Foyel Group (Feruglio, 1941; Diez & Zubia, 1981; Ramos, 1982; Barreda et al., 2003; Asensio et al., 2005, 2010; Bechis et al., 2014b). The eastern depocentres are part of the Ñirihuau Basin, located between 41° and 43°30' S at the eastern slope of the Patagonian Andes (Figure 1A; Giacosa & Heredia, 1999). This basin is elongated, N to NW, probably influenced by the previous basement structures (Bechis & Cristallini, 2005). It is also markedly asymmetrical, with the principal depocentres located at its western border (Giacosa et al., 2005). Its infill is characterised by volcanic and sedimentary rocks included in the Nahuel Huapi Group, of Oligo-Miocene age, comprising the Ventana, Ñirihuau and Collón Curá formations (Cazau et al., 1989, 2005; González Bonorino & González Bonorino, 1978; Bechis et al., 2014b, 2015; Ramos et al., 2015; Butler et al., 2020). In the Early to Middle Miocene, it records a transition from initially extensional to syn-orogenic tectonic conditions (Mancini & Serna, 1989; Bechis & Cristallini, 2006; Asensio et al., 2008; Bechis et al., 2014b; Orts et al., 2015; Santonja et al., 2021).

The subject of this research is the Ñirihuau Formation, which was first characterised by Roth (1922) and was formally defined by González Bonorino (1973). It constitutes part of the clastic and volcanoclastic infill of the Ñirihuau Basin, located south-east of San Carlos de Bariloche

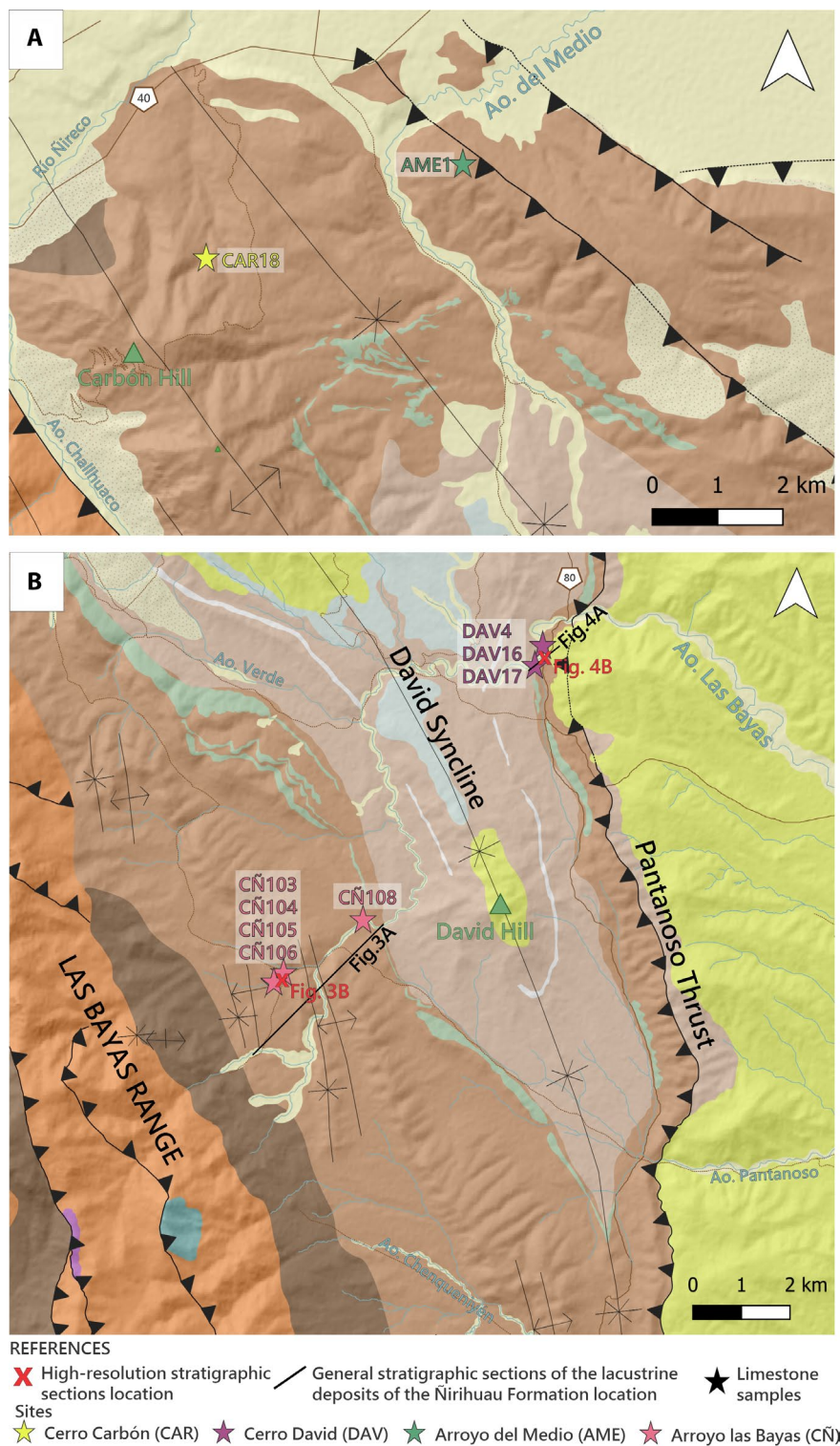
city (Figure 1; Cazau, 1972; Giacosa et al., 2001; Bechis et al., 2014b). Its thickness varies across the basin, reaching a maximum of 3500 m of well-stratified sediments to the east of the Las Bayas Range (Figure 1B; Mancini & Serna, 1989; Bechis, 2004; Santonja et al., 2021). According to available U–Pb geochronological data, this unit is Early to Middle Miocene in age (22–11.5 Ma; Ramos et al., 2015; Butler et al., 2020; Santonja et al., 2021). The Ñirihuau Formation was interpreted as deposited in alluvial, lacustrine, deltaic and fluvial environments (Cazau, 1972, 1980; Spalletti, 1981; Cazau et al., 1989; Mancini & Serna, 1989; Giacosa et al., 2005; Paredes et al., 2009; Ramos et al., 2011; Santonja et al., 2021). However, based on sedimentary structures that suggest tidal influence (Spalletti, 1981, 1983; Asensio et al., 2004), on the appearance of marine microfossils (dinoflagellates and acritarchs) found in exploration well samples (Cazau et al., 1989) and on the discovery of marine molluscs (González Bonorino & González Bonorino, 1978; Ramos, 1982), a connection to the sea during deposition of its middle section was proposed. Nevertheless, the existence of a freshwater environment is evidenced by osseous fish, crustacea and ostracods found in different mudstone levels of the lacustrine facies (Bocchino, 1964; Aragón & Romero, 1984; Pascual et al., 1984; Cazau et al., 1989; Aguirre-Urreta, 1992; Bertels & Cusminsky, 1995; Cione & Báez, 2007). Abundant remains of fossil flora were identified in the Ñirihuau Formation, including dicotyledons from the *Nothofagus* flora, that would have flourished under a temperate to warm temperate and humid climate, with drier conditions towards the top of the unit (Aragón & Romero, 1984; Passalia & Bechis, 2012; Falaschi et al., 2012; Caviglia & Zamaloa, 2014; Passalia et al., 2019; Caviglia, 2018).

In the northern sector of the basin, which is the focus of this study (Figure 1B), the Ñirihuau Formation is deformed by shallow thrusts and related folds (González Bonorino & González Bonorino, 1978; Bechis, 2004; Giacosa et al., 2005). In particular, the broad David Syncline (Figure 1B) was formed during the compressive deformation of the northern sector of the basin, which took place during the final stages of deposition of the Ñirihuau Formation (Paredes et al., 2009), in response to the Miocene Andean uplift (Santonja et al., 2021).

3 | STRATIGRAPHIC FRAMEWORK

The most complete and continuous section of the Ñirihuau Formation (around 3500 m thick) is exposed along the Arroyo Las Bayas in the western flank of the David Syncline (Figure 2B), where it was divided into three different informal units: lower, middle and upper sections

FIGURE 2 (A) Detailed geologic map showing the location of the limestone beds sampled (yellow and green stars) at Cerro Carbón (CAR) and Arroyo del Medio (AME). (B) Detailed geologic map of the Arroyo Las Bayas area, showing the location of the limestone beds sampled (pink and violet stars) and of the detailed stratigraphic sections surveyed and studied in this contribution for the Nirihuau Formation middle section (red crosses) at the eastern and western flank of the David Syncline, at Arroyo Las Bayas and Cerro David (CÑ and DAV, respectively) where the limestones samples were collected. See Figure 1 for map location and further cartographic and geologic references.



(Santonja et al., 2021). The lower section is constituted by amalgamated lenticular conglomerate bodies with interbedded volcanic rocks and, in lower proportion, sandstones. They were interpreted as deposited on a medial to distal alluvial fan or an axial fluvial system developed in the most distal part of an alluvial fan. The middle section of the unit has two thick intervals of lacustrine deposits, separated by a Gilbert-type delta (Figure 3A). The older

lacustrine system is made up of fine-grained deposits and extensive extensional syndepositional features. In contrast, the younger lacustrine system (above the deltaic deposits) exhibits a greater areal extent than the older one, but similar to thinner vertical thicknesses of fine-grained facies that contain microfossils that could indicate a brief connection to the sea during deposition (Mancini & Serna, 1989; Cazau et al., 1989). Most of the limestone beds studied are

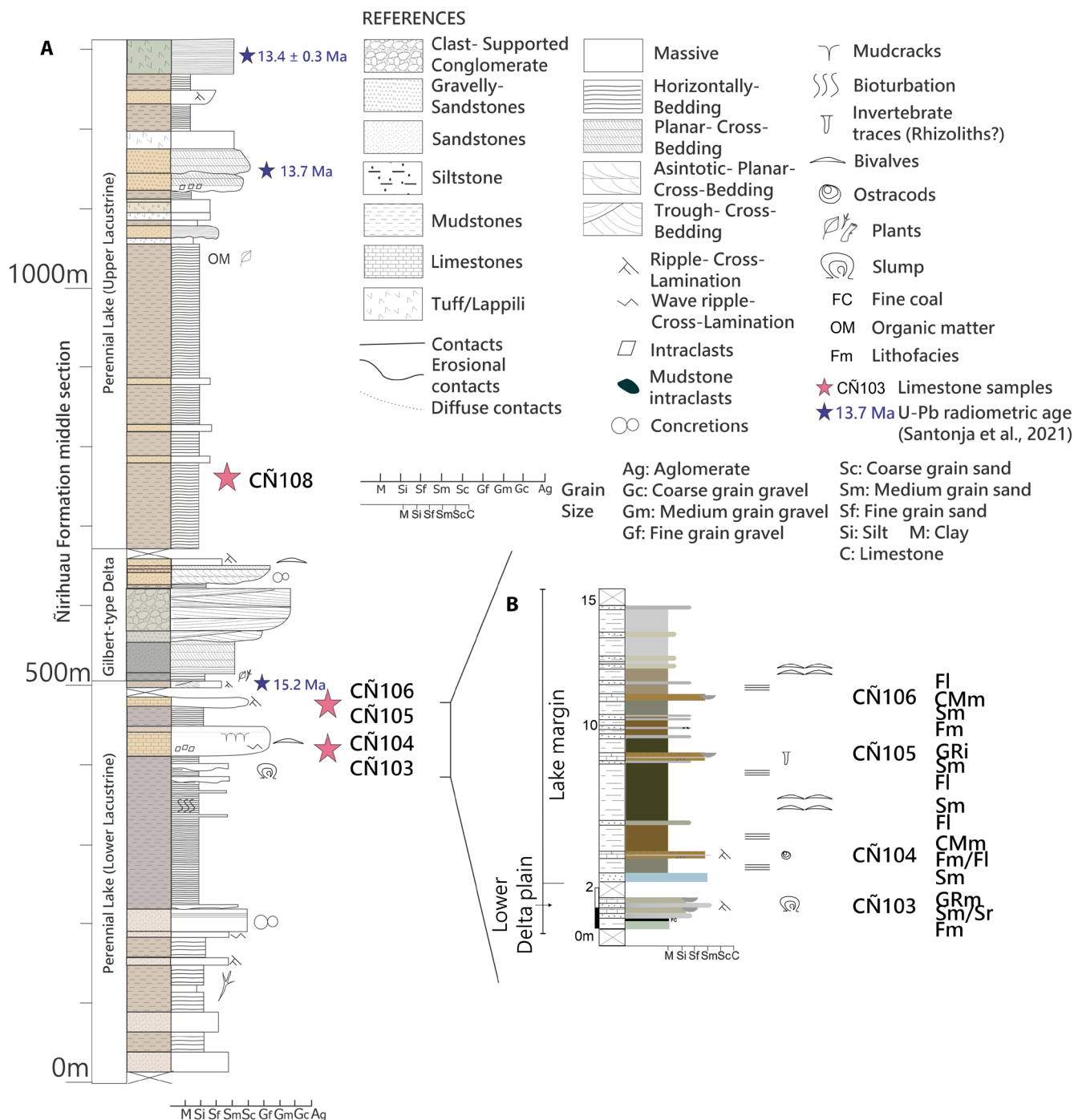


FIGURE 3 (A) Synthetic stratigraphic section of the Ñirihuau Formation middle section along the Arroyo Las Bayas at the western flank of the David Syncline (Arroyo Las Bayas), based on Santonja et al. (2021). The colour of the lithology column represents the colour of the deposits. Previously acquired U/Pb LA-ICP-MS geochronology data are also included (Santonja et al., 2021). Vertical scale 1:2000. (B) Detailed stratigraphic section of the Ñirihuau Formation middle section where the limestone beds were identified (CÑ section). The colour of the beds reflects the colour of the deposits. Vertical scale 1:200. See Figure 2B for the location of the surveyed sedimentary log. See Table 3 for microfacies classification of the limestone samples.

exposed in the uppermost portion of the older lacustrine interval (Figure 3A) and only one limestone bed was observed in the younger lake interval. Finally, the upper section of the Ñirihuau Formation contains deposits of higher energy with syndimentary deformation, interpreted as

sandy braided and anastomosed fluvial systems, with both braided and meandering channels, and extensive development of muddy floodplains (Santonja et al., 2021).

The lacustrine succession along the Arroyo Las Bayas on the eastern flank of the David Syncline, named in this

contribution as the Cerro David site (Figure 2B) shows some differences from the succession in the west. It is about 300m thick and contains tabular grey to light green siltstones and mudstones with interbedded sandstones, limestones and, subordinately, tuffs. Biological activity is registered on the finer-grained deposits as bioturbation is observed on some beds. The sandstone intervals are variable in thickness and

spacing, in most cases with irregular bases and lenticular geometry. Their abundance and grain size increase towards the top. Conversely, the limestone beds are restricted to the first 50m of the succession, which is the section studied in this contribution (Figure 4A).

Isolated limestone beds have been observed in the middle Ñirihuau Formation at the Cerro Carbón and

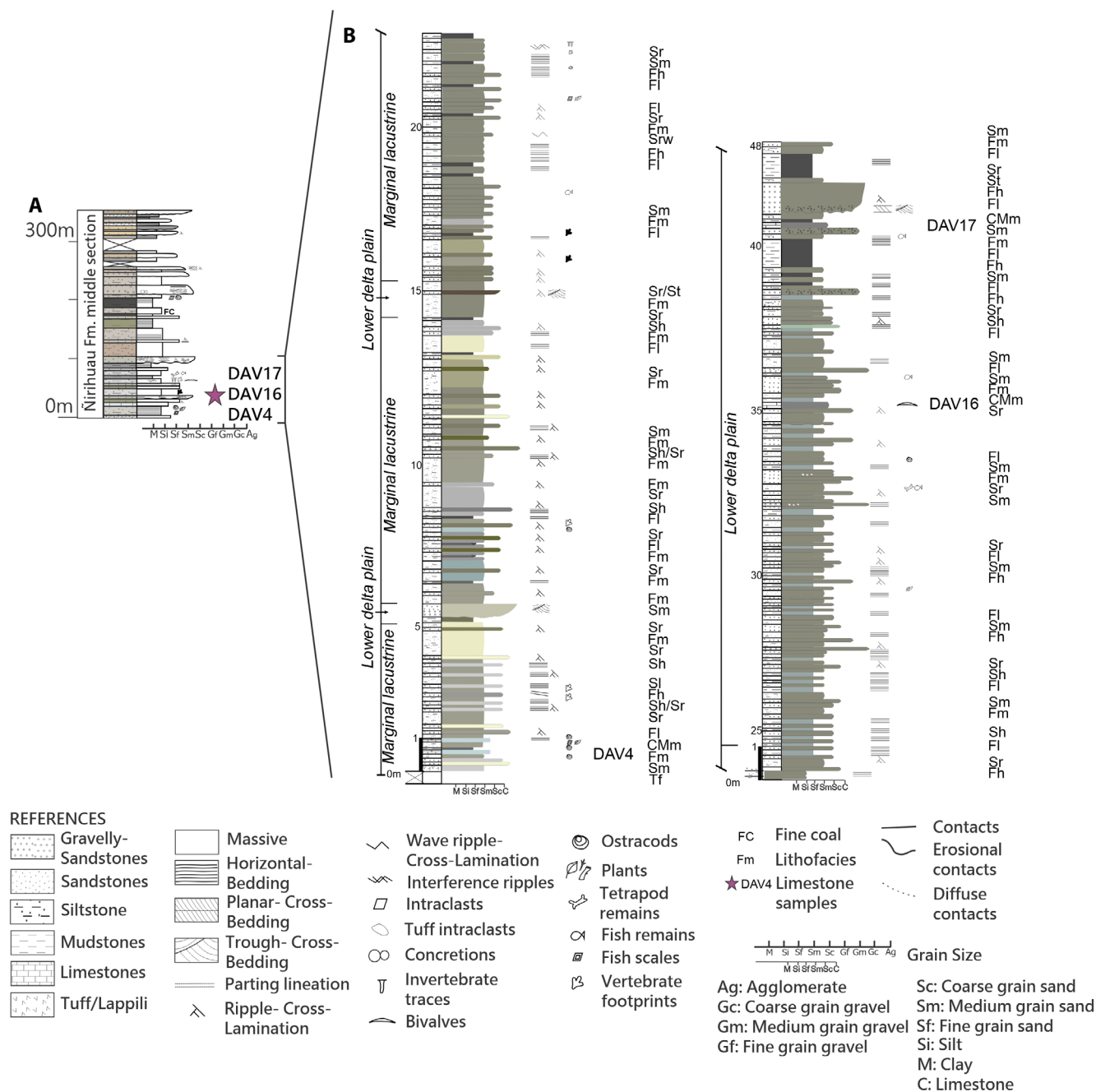


FIGURE 4 (A) Synthetic stratigraphic section of the Ñirihuau Formation middle section along the Arroyo Las Bayas at the eastern flank of the David Syncline (Cerro David site). The colour of the lithology column represents the colour of the deposits. Vertical scale 1:2000. (B) Detailed stratigraphic section of the middle Ñirihuau Formation where the limestone beds were identified (DAV site). The colour of the beds reflects the colour of the deposits. Vertical scale 1:200. See Figure 2B for the location of the surveyed sedimentary log. See Table 3 for microfacies classification of the limestone samples.

Arroyo del Medio sites (Figure 2A), which are located in the northernmost sector of the basin. However, no stratigraphic section was described at those sites. At Cerro Carbón, the limestone bed is interbedded with siliciclastic deposits represented by brownish medium-grained to fine-grained sandstones with tractive flow sedimentary structures and mudstones. At Arroyo del Medio, the limestone bed is interbedded with siliciclastic deposits consisting of green-coloured structureless mudstones and light-brown to green-coloured fine-grained

sandstone beds 10 cm thick, with erosive bases and horizontal lamination, ripple-cross lamination or a structureless appearance.

4 | METHODS

A 48 m and a 15 m thick stratigraphic log of the middle section of the Ñirihuau Formation was surveyed in detail along the Arroyo Las Bayas (Figure 2B), at the western and eastern

TABLE 1 Lithofacies identified along the detailed stratigraphic sections of the Ñirihuau Formation (Miocene), Ñirihuau Basin, Patagonia, Argentina. Modified from Miall (1996).

Code	Description	Process
Fm	Structureless mudstone	Low regime fluid flow, decantation by flocculation or bioturbation
Fl	Laminated mudstone	Low regime fluid flow, suspension settle out or decantation processes
Fh	Laminated siltstone	Low regime fluid flow, suspension settle out or decantation processes
Fb	Bioturbated siltstone	Organism activity
Sm	Structureless sandstone	Hyperconcentrated gravitational flow or low regime fluid flow with a sudden loss of energy and quick deposition
Sh	Horizontally bedded sandstone	Low/high regime fluid flow (medium- to coarse-grained sandstone) (tractive flow)
Shh	Horizontally bedded sandstone with parting lineation	High regime fluid flow (fine-grained sandstone) (tractive flow)
Sl	Low-angle cross-laminated sandstone	Unidirectional low regime fluid flow (tractive flow)
Sr	Ripple cross-laminated sandstone	Unidirectional low regime fluid flow (tractive flow)
Srw	Wave ripple cross-laminated sandstone	Bidirectional low regime fluid flow (tractive flow)
Sp	Planar cross-bedded sandstone	Unidirectional low regime fluid flow (tractive flow)
St	Trough-cross-bedded sandstone	Unidirectional low regime fluid flow (tractive flow)
GRI	Grainstone with intraclast	Tractive flow
GRr	Ripple cross-laminated grainstone	Unidirectional low regime fluid flow
GRrw	Wave-ripple cross-laminated grainstone	Bidirectional low regime fluid flow
GRh	Horizontally laminated grainstone	Low regime fluid flow
GRht	Heterolithic grainstone	Low regime fluid flow with tidal influence
GRT	Trough-cross-bedded grainstone	Unidirectional low regime fluid flow
GRm	Structureless grainstone	Low-energy conditions
CMm	Structureless calcimudstone	Low-energy conditions
Tf	Tuff	Volcanic activity synchronous with sedimentation
FC	Fine coal	Production and accumulation of transported organic material

flanks of the David Syncline, respectively (Arroyo Las Bayas and Cerro David sites, [Figures 3 and 4](#)). They were chosen due to outcrop quality, with limestone beds interbedded within the fine-grained deposits. The sections were characterised according to lithology, colour, sedimentary structures, bed geometries and fossil content. The Rock Colour Chart of the Geological Society of America (GSA; Goddard et al., 1948) was used for descriptions. Limestone beds were described in the field following the Dunham classification (Dunham, 1962) modified by Wright (1992). Lithofacies were identified and named, modifying the code of Miall (1978; [Table 1](#)) based on lithological characteristics and sedimentary structures. The lithofacies, which indicate sedimentary processes according to Miall (1996), were grouped into facies, to interpret the depositional sub-environment. These facies were then grouped into facies associations, in order to interpret the depositional palaeoenvironment and construct a facies model of the analysed successions as described by Posamentier and Walker (2006 and references therein; [Table 2](#)).

A total of 10 hand samples were collected from the limestone beds at Arroyo Las Bayas and Cerro David (southern David Syncline) and at Cerro Carbón and Arroyo del Medio (northern David Syncline) for further petrographic and geochemical analyses ([Figure 2](#); [Table 3](#)). Carbonate was determined in hand samples by HCl reaction and calcite with Alizarin Red-S stain. The samples were chosen to be representative of all the different macrofabric features identified in the field. They were named with an abbreviation of the location (DAV for the Cerro David site, CÑ for the Arroyo Las Bayas site, CAR for the Cerro Carbón site and AME for the Arroyo del Medio site) plus a consecutive number ([Figure 2](#)). Thin sections of hand samples were studied using a petrographic microscope (Olympus BX-51) at the Laboratorio de Paleontología from the Instituto Argentino de Nivología, Glaciología y Ciencias Ambientales (IANIGLA), in Mendoza City, Argentina. They were described according to the carbonate fabric features, and the petrographic classification followed Gierlowski-Kordesch (2010) for carbonate microfacies. Criteria to differentiate primary carbonate from different diagenetic carbonate phases included a thorough multiproxy study with petrography and cathodoluminescence (Murphy et al., 2014; Henkes et al., 2018; Parrish et al., 2019; Benavente et al., 2019).

Cathodoluminescence analysis was conducted on seven of the samples at the Laboratorio de Luminiscencia of the Departamento de Geología from the Universidad Nacional del Sur (UNS), in Bahía Blanca City, Argentina ([Table 3](#)). For this purpose, 30 µm thick thin sections were prepared from each sample. A Nikon Eclipse 50iPol polarisation and fluorescence microscope with a CITL Mk5 cathodoluminescence stage was used. This stage has a vacuum chamber and contains the sample which was

TABLE 2 Facies and facies association recognised along the detailed stratigraphic sections of the Ñirihuau Formation (Miocene), Ñirihuau Basin, Patagonia, Argentina, with their main characteristics. The proportions of the different lithologies are indicated in approximate percentages to reflect their abundance. Goddard et al. (1948) Rock Colour Chart of the Geological Society of America codes are indicated next to each lithofacies between brackets.

Facies association	Characteristics	Facies	Facies interpretation	Facies association interpretation
FA1: Mudstones and siltstones with interbedded limestones and sandstones	Up to 70 m thickness of alternating tabular mudstone and siltstone beds with intercalations of tabular limestone beds and tabular to lenticular channelised sandstone bodies of variable thickness and frequency. Organic activity present. (S: 30%; F: 50%; Limestones: 20%; T: <1%; FC: <1%)	Facies 1: Sm (5Y6/1 - 5B7/1 - 5B5/1 - N8 - 5YR6/1 - 5YR4/1 - 5Y8/1 - 10YR8/2 - 10Y6/2), Sh (N6 - N8), Sl (N6), Sr (5Y6/1 - 5Y5/2 - 10Y4/2 - N7 - 5GY5/2 - 5GY3/2 - 5YR4/1), Srw, Fm (5Y4/1 OLIVE GREY - 5Y3/2 - 5Y7/2 - 5B7/1 - 5GY6/1 - N7 - N5 - 5GY5/2), Fl (10YR4/2 - 5YR4/1 BROWNISH GREY - N7 - 10YR6/2 - 5Y6/1 - 5Y5/2), Fh, Fb, Cmm (5Y6/1), GRi, GRt, GRrw, GRh, GRht, Tf (5B7/1 LIGHT BLuish GREY) (S: 30%; F: 50%; T: <1%; Limestones: 20%)	Marginal lacustrine	Perennial lake associated with a deltaic system and dominated by fluvial input
		Facies 2: St, Sr, Sm (5Y4/1 - 5Y6/1), Sh, Fl, Fm (10YR4/2 - 10YR6/2), Fh, Cmm, GRm, FC (S: 40%; F: 50%; Limestones: 10%; FC: <1%)	Lower delta plain	

irradiated with an electron beam. Analytical conditions were 0.005 mBar with 15 Kv under about 250 μ A. This study allowed the identification of different cementation events and the assessment and estimation of Mn and Fe content of individual calcite crystals by colourimetry (comparison with published luminescence standards of known concentrations; Machel, 2000). In general, calcite enriched in Mn presents high luminescence and is an indicator of secondary enrichment (Parrish et al., 2019), whereas the response is subdued if it contains Fe, which can be considered a suppressor (Marshall, 1988; Mariano, 1988).

Eight calcitic carbonate samples were selected for carbon and oxygen stable isotope analysis, $\delta^{13}\text{C}$ and $\delta^{18}\text{O}$ (Table 3). A micro-drill was used to separate primary precipitated micrite with the intention of obtaining indicators of palaeoenvironmental conditions. Samples were analysed on a Thermo Fisher Scientific GasBench II, with a PAL autosampler, a ConFlow IV interface and a MAT 253 mass spectrometer (Thermo Fisher Scientific) at the Stable Isotope Ratio Facility for Environmental Research (SIRFER), University of Utah, Salt Lake City, Utah, USA. Internal reference materials (Carrara marble, LSVEC and Marble-Std) were calibrated against international standards NBS-18 and NBS-19. The oxygen fractionation factor was calculated using the alpha value proposed by Swart et al. (1991). Values are reported as *per mil* relative to the Vienna Pee Dee belemnite (VPDB) standard. Precision was better than 0.05‰ for $\delta^{18}\text{O}$ and 0.02‰ for $\delta^{13}\text{C}$. The data obtained were analysed statistically with the InfoStat 2020 software to determine sample distribution, and the Shapiro–Wilk and Pearson tests were performed.

5 | SEDIMENTOLOGY

5.1 | Facies analysis and depositional palaeoenvironments at Arroyo Las Bayas stratigraphic sections (CÑ and DAV sites)

The palaeoenvironmental analysis is based on the two detailed stratigraphic sections surveyed along the Arroyo las Bayas. The CÑ section focussed on the limestone beds recognised within the lacustrine facies as described by Santonja et al. (2021; Figure 3). The Cerro David site (DAV), surveyed in this work, yielded a detailed stratigraphic section of the carbonate-rich deposits of the lacustrine facies (Figure 4). One facies association (FA 1) was defined based on these two sections to represent the depositional palaeoenvironment. Within this facies association, two facies were interpreted, meaning two different subenvironments were recognised.

5.1.1 | FA 1: Mudstones and siltstones with interbedded limestones and sandstones

Description

This facies association exhibits substantial volumes of mudstones and siltstones with interbedded limestone and sandstone beds of variable thicknesses, spacing and abundance. A volcanic intercalation occurs at the base of the stratigraphic section at DAV. FA 1 comprises two facies (Facies 1 and 2; Table 2) according to the predominance of different lithologies and their characteristics.

Facies 1 occurs in the uppermost part of the stratigraphic section at CÑ and in the lowermost portion at DAV (Figures 3 and 4). This facies exhibits a great thickness of thinly interbedded light green to grey ostracod-bearing siltstones and dark grey mudstones, with sandstones and some limestone beds (Figure 5A). The mudstone and siltstone beds are tabular, both laminated (Fl, Fh) and structureless (Fm). Tetrapod tracks occur at some levels of the succession (Figure 5D). Plant remains, bioturbation (Fb), bivalves, fish scales and osseous remains were frequently observed in these deposits (Figure 5E,F). The interbedded sandstones occur as thin tabular beds, 5–15 cm thick, with erosional or planar bases displaying various sedimentary structures (Sh, Shh, Sl, Sr, Srw or Sm). The limestones, at DAV are tabular beds of structureless calcimudstones (CMm, sample DAV4), ranging from 5 up to 10 cm thick, with planar bases, whereas those at CÑ consist of tabular to lentiform beds, from 30 to 10 cm thick, with planar or erosive bases of grainstones (sample CÑ105) and calcimudstones (samples CÑ104 and CÑ106). Grainstones contain intraclasts (GRi), and different types of lamination (GRht, GRh, GRr, GRrw), whereas calcimudstones are mainly structureless (CMm) or have synsedimentary deformation (convoluted lamination and mudcracks; Figure 6). These limestone beds contain bivalve fossils, assigned to the freshwater mussels *Diplodon* sp. (see Santonja et al., 2021), and also undetermined ostracod remains. These ostracods are mostly disarticulated and generally poorly preserved and exhibit a thin shell wall typical of freshwater forms. Finally, a 10 cm thick tuff bed (Tf) was observed at the base of the stratigraphic section at DAV.

Facies 2 is observed interbedded with Facies 1. At CÑ Facies 2 was recognised only in the lowermost part of the section, whereas at DAV, it occurs repeatedly in the section (Figures 3 and 4). Facies 2 consists of grey sandstones interbedded with grey siltstones and mudstones (Figure 5G,H). Subordinate limestone beds and coal layers were observed. The finer grain deposits are light to dark green, grey and occasionally brown mudstones and siltstones with thin lamination (Fl and Fh, respectively) or a structureless appearance (Fm). They range in thickness

TABLE 3 Analyses conducted on the different carbonate samples of the Ñirihuau Formation (Miocene), Ñirihuau Basin, Patagonia, Argentina. If an analysis has not been conducted for the sample, it is indicated with the em dash (—).

Site	Sample	Microfacies	StL/F	Petrography and Diagenetic zone	Cathodoluminescence and Diagenetic stage	Stable isotopes	
						$\delta^{13}\text{C}$ VPDB	$\delta^{18}\text{O}$ VPDB
Arroyo Las Bayas	CÑ103	Intraclastic grainstone	F2	Circumgranular spar rim— <i>Meteoric phreatic</i>	Micrite, fibrous calcite cement, and euhebral spar crystals; reddish dark weak luminescence. Clasts: non-luminescent <i>Eogenesis</i>	−4.0	−14.1
	CÑ104	Homogeneous calcimudstone	F1	Bladed spar meniscus cement— <i>Meteoric vadose and phreatic</i>	Homogeneous micrite matrix: moderate luminescence Cracks: margin with dark orange dull luminescence bladed calcite rim (meniscus cement); centre with dark brown dull luminescence granular spar mosaic. Bladed calcite with bright luminescence around clasts within cracks <i>Eogenesis</i>	−2.4	1.1
	CÑ105	Silty grainstone	F1	Crenulated layers and radial tubules of microspar	—	—	—
	CÑ106	Disrupted micrite	F1	Blocky spar— <i>Meteoric vadose and/or phreatic</i>	Homogeneous to grumous micrite matrix: dull luminescence. Fenestrae: moderate luminescence microspar Valves and cracks: non-luminescent blocky mosaic spar. Siliciclasts: Bright orange luminescence (carbonate corrosion) <i>Eogenesis</i>	8.5	−3.1
Cerro David	CÑ108	Birds eye micrite	—	Disruptive structures with microspar margins	—	14.2	0.1
	DAV4	Bioclastic mudstone	F1	Fibrous spar— <i>Meteoric vadose</i> Acicular calcite cement— <i>Mixing meteoric marine</i>	Siliciclastic fine-grained matrix: non-luminescent Microfractures, cement, and bioclasts: moderate luminescence fibrous spar and calcite acicular overgrowth <i>Eogenesis</i>	—	—
	DAV16	Calcimudstone with sparse detrital grains	F2	Isopachous calcite cement rim— <i>Possibly meteoric</i>	Grumous micrite matrix: dull brown to non-luminescent Fractures: weak to non-luminescence spar (isopachous rims). Cracks: bright orange luminescence Spartic valves and siliciclastic grains: non-luminescent. <i>Eogenesis</i>	2.7 1.0	−11.7 −7.1
	DAV17						
Cerro Carbón	CAR18	Fenestral micrite	—	Blocky spar— <i>Meteoric vadose and/or phreatic</i>	Grumous micrite and patches blocky of spar cement: bright orange luminescence Valves and siliciclastic grains: dark brown dull to non-luminescent Fenestrae: microcrystalline quartz <i>Eogenesis</i>	3.3	−15.6

(Continues)

TABLE 3 (Continued)

Site	Sample	Microfacies	StL/F	Petrography and Diagenetic zone	Cathodoluminescence and Diagenetic stage	Stable isotopes	
						$\delta^{13}\text{C}$ VPDB	$\delta^{18}\text{O}$ VPDB
Arroyo del Medio	AME1	Stromatolitic boundstone	—	Fibrous spar—Meteoric vadose Circumgranular spar rim— <i>Meteoric phreatic</i>	Grumous/mottled micrite matrix, spar mosaics, circumgranular spar rim, and fibrous spar: moderate orange luminescence Sparitic valves and other bioclasts: dark orange weak luminescence. Fractured feldspar crystals with a bright luminescent cement Fibrous spar layers: alternating medium and low luminescence Crack margins with dense micrite: dull luminescence. Microstylolites: non-luminescent <i>Eogenesis–Mesogenesis</i>	–3.5 –3.2	–15.6 –15.3

Abbreviations: StL/F, Stratigraphic log/Facies; VPDB, Vienna Pee Dee belemnite standard.

from 10 cm to 10 m, and contain fish remains. The sandstone beds are mainly lenticular with erosive bases, range between 20 cm and 90 cm thick and contain coarse to medium sand grains. They contain muddy intraclasts and an internal decreasing grain size trend towards the top. The sedimentary structures observed are trough cross-stratification (St), ripple cross-lamination (Sr), horizontal lamination (Sh) and structureless (Sm). Very scarce limestone beds are interbedded with the fine-grained deposits (Figure 5B). They consist of calcimudstones and grainstones, and are observed as laterally discontinuous bodies 10 cm thick with a structureless appearance (CMm and GRm, samples DAV16, DAV17 and CN103). Also, a coal layer a few centimetres thick (FC), was observed intercalated with the siltstones at the lowermost portion of the CN stratigraphic section.

Interpretation

Facies 1 is interpreted as having accumulated in a marginal lacustrine zone. The intercalations of tabular bodies of siltstones, mudstones and sandstones in almost equal proportions are evidence of coastline fluctuations in a low-energy environment (Reading, 1996; Paredes et al., 2009). These deposits result from settle-out processes (Fm), and low-flow-regime transport (Fl, Fh, Sh, Sl, Sr) and, in some cases, from oscillatory flows (Srw) and high-flow-regime transport (Shh; Collinson & Thompson, 1989). Tetrapod tracks indicate shallow conditions and a well-oxygenated environment is also evidenced by the presence of a great variety of biological activity, such as bivalves, ostracods and bioturbation. Furthermore, the presence of wave ripple lamination (Srw) indicates that the deposition occurred above the wave base (Nichols, 2009).

Facies 2 is interpreted as deposited in a lower delta-plain environment, where the distributary channels are preserved as lenticular sandstone bodies with tractive flow structures (St, Sr, Sh, Sm) (Harms et al., 1982; Link et al., 1978). The overbank or inter-channel areas, sites of sedimentation of suspended load fallout when the channels flood, are preserved as tabular bodies of sandstones, siltstones and mudstones, with low-energy structures (Fl, Fh, Sm, Sh) (Arche, 1992; Reading & Collinson, 1996; Bhattacharya, 2006). This interpretation is reinforced by the presence of coal, as a product of the production and preservation of organic matter (OM) in shallow, low-energy swampy environments (interdistributary bay; Nichols, 2009). Although limestone beds are still observed in this facies (CMm), they are less abundant than in Facies 1 and sandstone intercalations are more plentiful, suggesting that the environment is closer to a source of clastic material that would come from fluvial input (Talbot & Allen, 1996). Facies 2 and

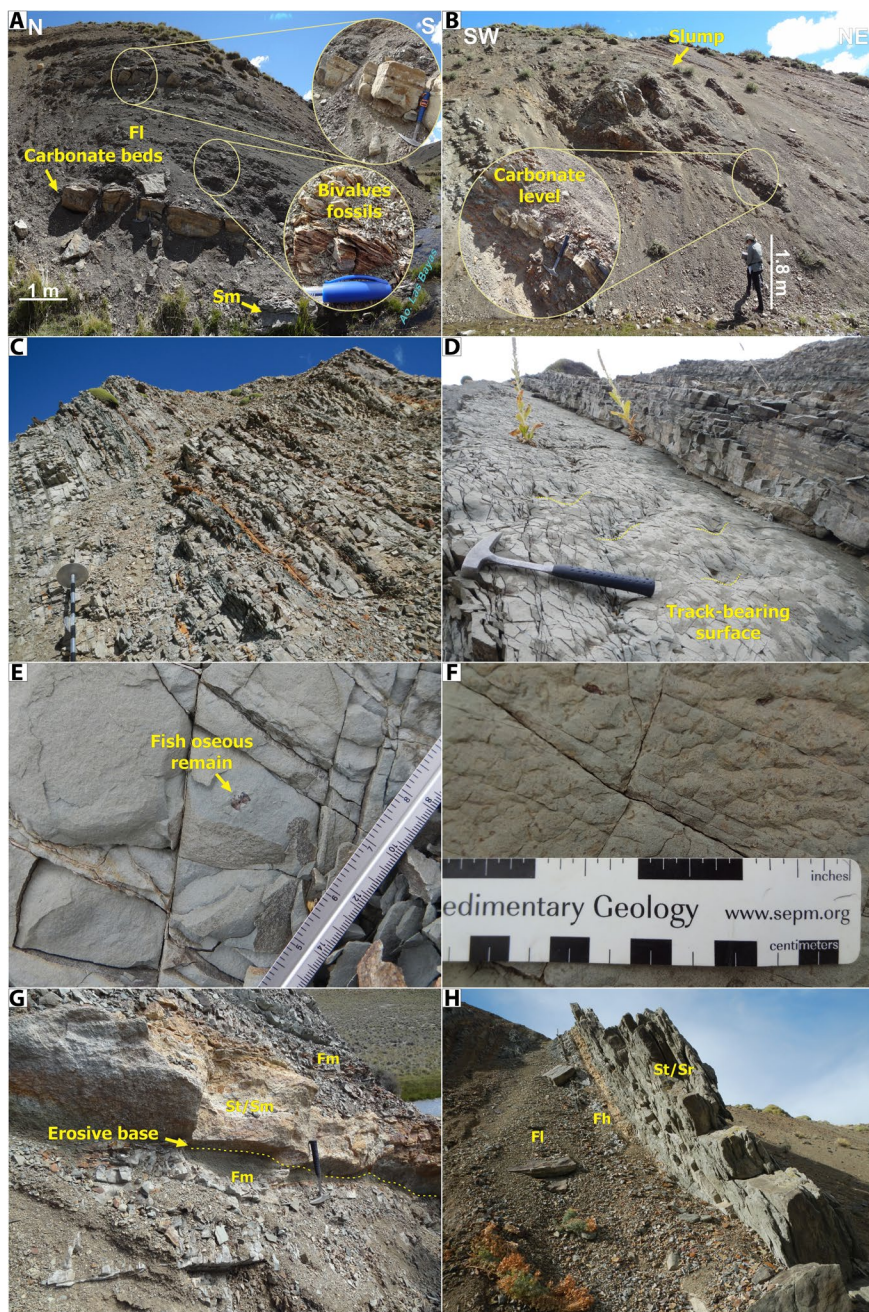


FIGURE 5 Field photographs of the sedimentary facies observed in the Ñirihuau Formation middle section. (A) CÑ stratigraphic section. Thinly interbedded light green to grey ostracod-siltstones, and dark grey mudstones, with sandstones and limestone beds of Facies 1. Lower inset shows bed containing bivalve fossils, upper exhibits ostracod-bearing limestone bed. (B) CÑ stratigraphic section. General view of the outcrop of Facies 2 affected by syndepositional deformation. Inset shows laterally discontinuous limestone beds interbedded among fine-grained deposits. (C) DAV stratigraphic section. Tabular deposits of mudstones and siltstones (Fl, Fh, Fm) with interbedded sandstones from Facies 1 of Facies Association 1. (D) DAV stratigraphic section. Tetrapod footprints preserved on siltstone beds of Facies 1. (E) DAV stratigraphic section. Detail of siltstone bed containing fish scales and skeletal remains abundant in Facies 1. (F) DAV stratigraphic section. Detail of bioturbated siltstone bed (Fb) from Facies 1. (G) DAV stratigraphic section. Grey sandstone bed interbedded with grey structureless mudstones and siltstones from Facies 2. (H) DAV stratigraphic section. Grey sandstone bed interbedded with light to dark green, grey and occasionally brown mudstone and siltstone with thin lamination from Facies 2.

Facies 1 are considered to have accumulated laterally to each other because they are generally observed to be interbedded.

Based on these observations, this facies association is interpreted to reflect a lacustrine environment associated with a delta plain, from a deltaic system. The predominance

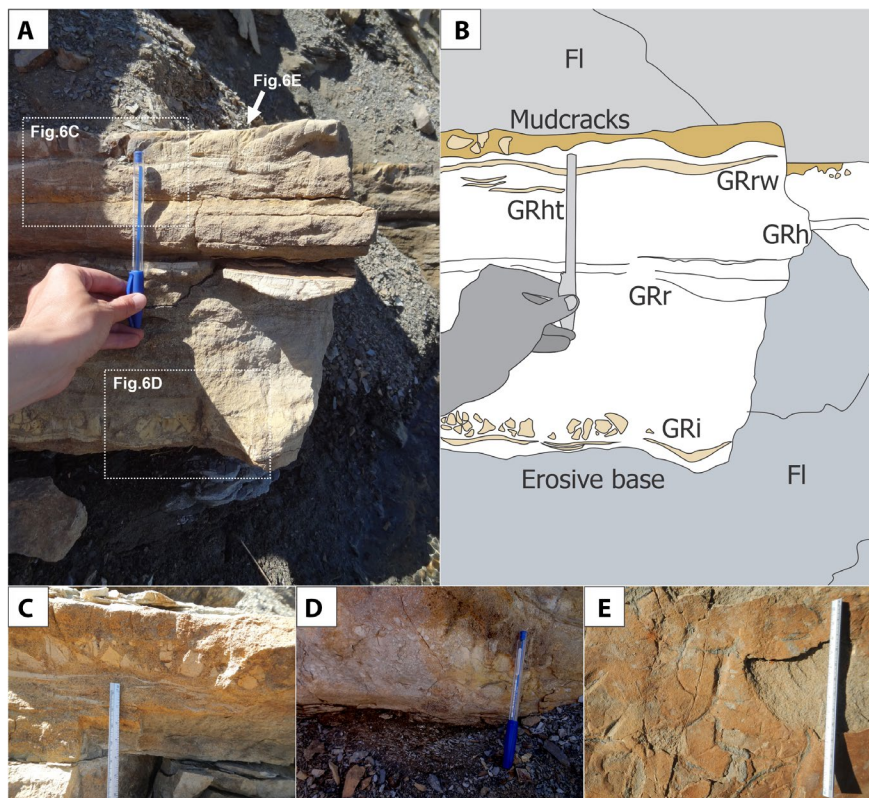


FIGURE 6 Field photographs of one of the limestone beds sampled from Facies Association 1 (Facies 1) from the CÑ stratigraphic section. (A, B) Limestone bed corresponding to sample CÑ104 and the recognisable sedimentary structures: intraclasts (GRi), heterolithic lamination (GRht), horizontal lamination (GRh), current-ripple cross-lamination (GRr) and wave-ripple cross-lamination (GRrw). FI: Laminated mudstones. (C) Details of the uppermost portion of the limestone bed with heterolithic lamination and angular intraclasts. (D) Details of base of limestone bed with intraclasts. (E) Details of top of the limestone bed with mudcracks and ochre colour, likely due to oxidation (plan view). See Figures 2 and 3 for the location of the stratigraphic section and sample.

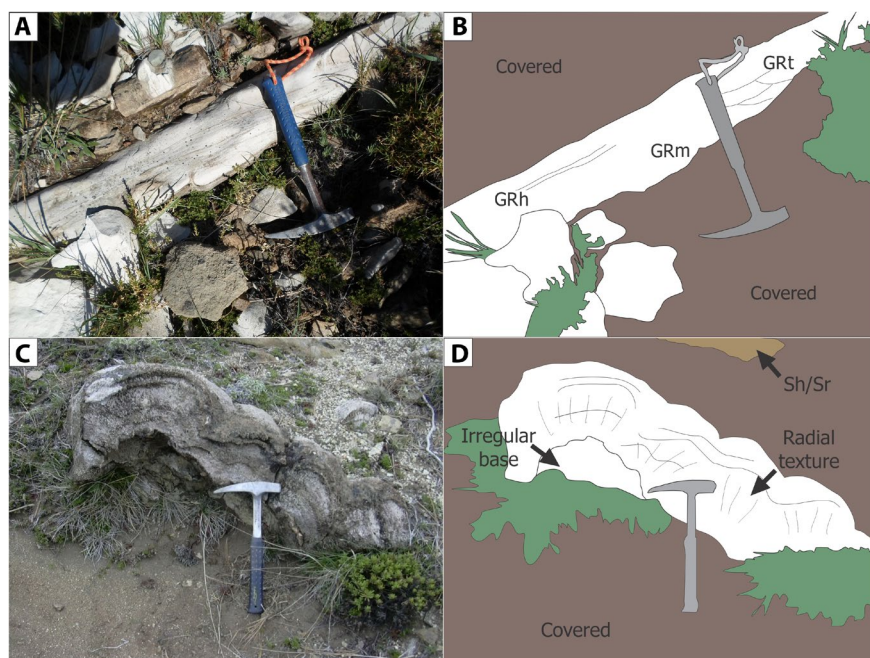


FIGURE 7 Field photographs of some of the limestone beds sampled. (A, B) Limestone bed from Cerro Carbón (corresponding to sample CAR18) and the sedimentary structures recognised on it: horizontal lamination (GRh), trough cross-bedding (GRt) and structureless (GRm). (C, D) Limestone bed with dome geometry, radial texture at the base and banded structure at the top from Arroyo del Medio (corresponding to sample AME1) interpreted as microbialites formed by bioinduced precipitation. The main features are indicated. See Figure 2 for the location.

of laterally continuous fine grain size deposits both laminated and structureless, with intercalations of sandstones and limestone beds suggest a nearshore lacustrine

palaeoenvironment with occasional fluvial influx, resulting in the formation of a delta where the river met the lake (Anadón, 1992; Talbot & Allen, 1996; Håkanson, 2007).

5.2 | Limestone beds at Cerro Carbón and Arroyo del Medio (CAR and AME sites)

Carbonate deposits occur as isolated beds in the northern part of the basin, at the Cerro Carbón and Arroyo del Medio sites. Since their macrofabric and microfabric differ significantly from the carbonates found to the south at the CÑ and DAV sites (see [Figures 1](#) and [2](#) for sites location; [Table 3](#) for macrofacies and microfacies sample references) their sampling and analysis provide crucial information about the entire Ñirihuau continental carbonate factory.

5.2.1 | Cerro Carbón site (CAR)

Description

The limestone bed has a tabular geometry ranging from 10 to 15 cm thick with a planar to slightly erosive base. It is a white-coloured grainstone with such sedimentary structures as horizontal lamination (GRh) and trough cross-lamination (GRt) or they may appear structureless (GRm) ([Figure 7A,B](#)).

Interpretation

The sedimentary structures observed in the limestone bed suggest transport of the carbonate material in sublittoral areas of a lake by low regime tractive flows. The structureless grainstones may have been generated through gravity flows or resuspension of sediments (Alonso-Zarza & Tanner, 2010).

5.2.2 | Arroyo del Medio site (AME)

Description

At Arroyo del Medio a 30 cm thick, dark-brown to grey-coloured limestone bed is exposed. It exhibits a domed geometry (Kennard & Burne, 1989) consisting of laterally linked hemispheroids, each about 30 cm high, 15 cm long and 20 cm wide (Bechis, 2004). The internal growth forms domes, which have an irregular base, radial texture at the base where lamina shapes are gently convex with non-enveloping margins, and a banded structure with slightly undulatory and laterally continuous laminae at the top ([Figure 7C,D](#)).

Interpretation

The domal carbonate structures with an internal aggrading fabric made up of laminae are interpreted as microbialites formed mainly by bioinduced precipitation (Awramik & Riding, 1988; Dupraz et al., 2009), and correspond to

laterally linked hemispheroids *sensu* Logan et al. (1964). The irregular base could be due to an uneven original substrate or to dissolution processes. The hemispherical structures indicate a moderate to low hydraulic energy subenvironment in shallow to intermediate water depths possibly protected by physical barriers from high-energy currents (e.g. sand bars; Grotzinger & Knoll, 1995; Druschke et al., 2009) within the photic zone because they are built by photo-dependent microorganisms (Dupraz et al., 2004; Bourillot et al., 2020) and reduced input of siliciclastic grains (Alonso-Zarza & Tanner, 2010).

6 | CARBONATE MICROFACIES

All the limestone beds sampled were analysed under the microscope and seven of the samples were selected for analysis by cathodoluminescence ([Table 3](#)). The microscopic study of the thin sections yields microfacies data which, in conjunction with the insights derived from cathodoluminescence analyses, provide key information on sedimentary and diagenetic processes.

6.1 | Microfacies: Intraclastic grainstone

Description

Grain-supported microfabric with subangular to subrounded sparitic intraclasts 472–1180 µm in size. Some of the intraclasts show evidence of corrosion-like irregular margins and a 27 µm thick layer of opaque coating material. They have a rim, with an internal micritic opaque fringe of 27 µm in thickness, and an external one of 27–272 µm in thickness ([Figure 8A](#)), of circumgranular calcite cement ([Figure 8B](#)) and also of crystalline texture of calcite with radial fibrous habit. Scarce intraclasts preserve micritic crenulated lamination. The spar crystals of the intraclasts are euhedral and vary in size between 120 µm and 240 µm. There are scarce angular siliciclasts of feldspars, quartz and volcanic lithic fragments 250 µm in diameter. Spar crystals up to 100 µm in size with clear contacts fill the interparticle space. There are also clasts with diagenetic silica of 200 µm. Some of the intraclasts are connected with the adjacent ones, leaving only an observable line of opaque material remaining. This may be attributed either to the loss of part of the external layer or because the rim precipitated after they came into contact. Cathodoluminescence analysis shows that the micrite, fibrous radial calcite cement and spar have reddish, very dark weak luminescence, whereas quartz or feldspar clasts are non-luminescent ([Figure 8C](#)).

Interpretation

The intraclasts are the result of tractive flows eroding and transporting carbonate deposits from their originally adjacent subenvironment (Gierlowski-Kordesch, 2010). This is a common carbonate element in shallow marginal lacustrine subenvironments (Platt, 1989; Gierlowski-Kordesch, 2010). Intraclasts most likely represent biogenically induced carbonate precipitation of micrite since some of them still preserve micritic crenulated lamination (Figure 8A; Dupraz et al., 2009; Gierlowski-Kordesch, 2010). The irregular margin of a few intraclasts indicates that transport was not significant (Reading & Level, 1996; Nichols, 2009). The coating of opaque material is interpreted as OM that accumulated after transportation, while the circumgranular calcite cement as the result of dissolution and reprecipitation of carbonate in a meteoric-phreatic environment (Flügel, 2010). The dull luminescence could indicate low Mn content (Machel, 2000) or Fe concentration above 200 ppm (Hiatt & Pufahl, 2014). The reddish to dark weak luminescence is indicative of anoxic pore waters (Hiatt & Pufahl, 2014).

6.2 | Microfacies: Homogeneous calcimudstone

6.2.1 | Description

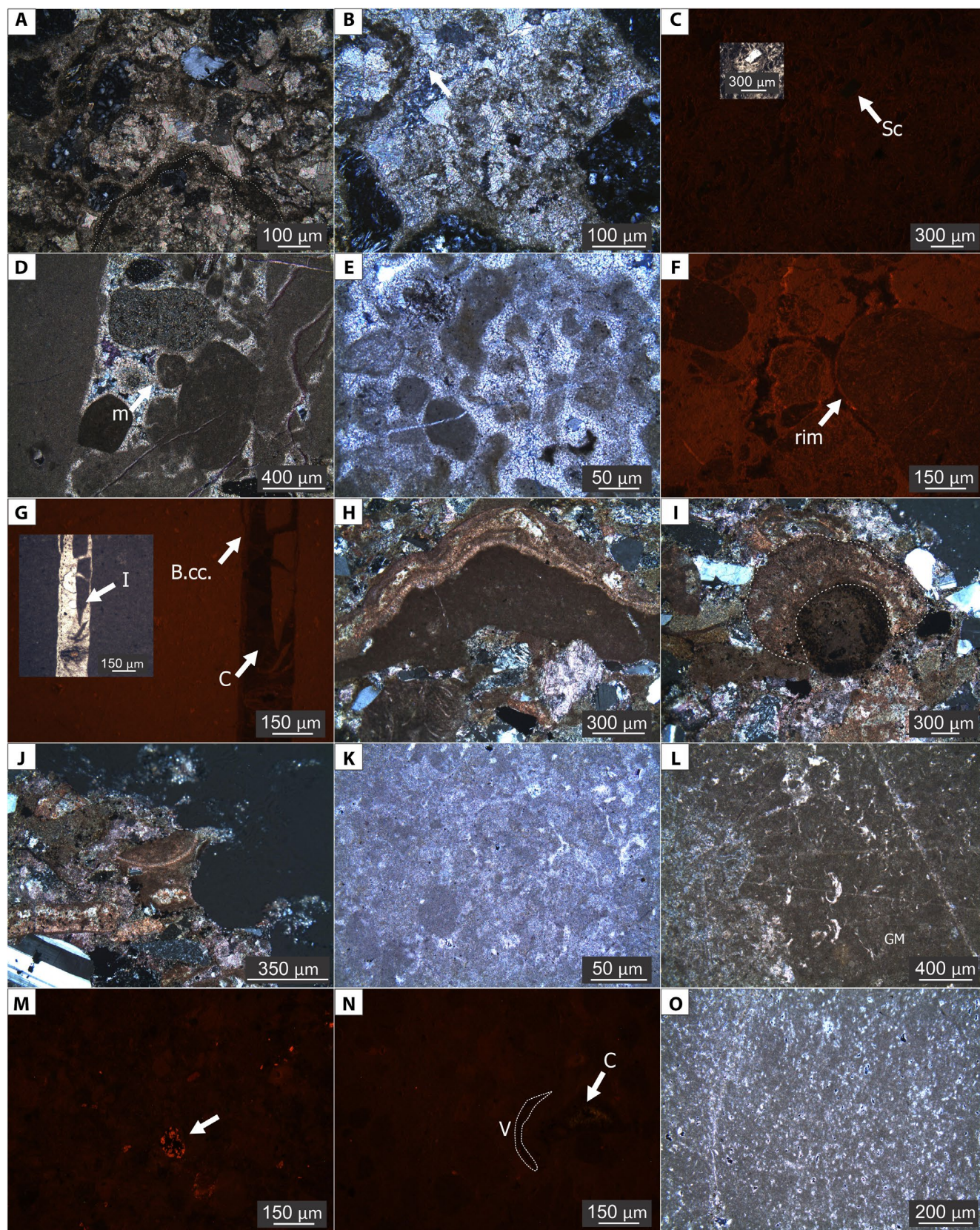
This microfacies comprises a homogeneous micrite matrix with vertical to subhorizontal cracks 1420 µm wide connected by thinner horizontal cracks 120–600 µm in width. The cracks have an isopachous rim of bladed calcite in their inner margin; they also contain 120–830 µm diameter, micritic subrounded and subangular intraclasts with

bladed calcite rims of 25 µm forming interparticle connections and granular calcite filling the remaining pores (Figure 8D). The spar crystals vary in size between 12 µm and 50 000 µm and form granular mosaics (Figure 8E). Within the cracks, there are also scarce angular grains of feldspars, quartz and lithic fragments 240 µm in diameter. The micrite matrix is moderately luminescent. The bladed calcite presents bright luminescence around clasts (Figure 8F) and dark orange weak luminescence in the inner margin of the cracks. The granular calcite has dark brown weak luminescence (Figure 8G). There are also bright luminescent thin veins affecting the cracks and non-luminescent silica cement was observed affecting the micritic matrix in a sector.

6.2.2 | Interpretation

The homogeneous micrite microfacies is interpreted as authigenic precipitation of carbonate in a subaqueous subenvironment (Schrug et al., 2013). The observed cracks have sharp margins and a different infilling than the matrix; therefore, they are interpreted as subaerial exposure cracks (Gierlowski-Kordesch, 1998). This implies the limestone bed records a shallowing upward trend, which is common in carbonate lacustrine ramp margins characterising a prograding trend (Figure 6; Platt & Wright, 1991; Tucker & Wright, 2002). Crack infilling is interpreted as carbonate grains eroded and transported from adjacent settings with moderate- to high-energy conditions (Platt & Wright, 1991) or perhaps shallower areas that had been desiccated (Gierlowski-Kordesch, 2010). The subrounded and subangular shape of carbonate grains points to the first option as the most plausible one. The bladed calcite

FIGURE 8 Microphotographs of some of the limestone beds sampled in the Ñirihuau Formation middle section at the CÑ stratigraphic section. (A) Grain-supported matrix of subangular to subrounded sparitic intraclasts (sample CÑ103). White dashed line indicates micritic crenulated lamination. (B) External layer of the circumgranular calcite cement rim (sample CÑ103). (C) Micritic matrix with homogeneous reddish very dark dull luminescence with non-luminescent siliciclast (sample CÑ103). Upper left corner shows the same siliciclast under parallel polarised light. (D) Homogeneous micrite matrix with vertical to subhorizontal wide cracks connected by thinner horizontal cracks (sample CÑ104). Isopachous rim of bladed calcite in inner margin, micritic subrounded intraclasts with bladed calcite rim (meniscus cement), and spar cement on the remaining vugs and voids of the cracks. (E) Granular mosaics of spar crystals (sample CÑ104). (F) Crack with angular siliciclasts of weak luminescence with a bright luminescent carbonate rim (sample CÑ104). (G) Homogeneous micritic matrix with weak orange luminescence disrupted by a crack with an inner margin of bladed calcite rim and subrounded micritic intraclasts, the remaining vugs of the crack are filled with a sparitic cement (sample CÑ104). Parallel polarised light picture shown on the left. Black dashed line indicates limit of bladed calcite and spar cement. (H) Grain-supported micrite grumous matrix of subangular to subrounded micrite intraclasts (sample CÑ105). A few contain horizontal laminae. (I) Scarce rounded intraclasts with faint tubules in a radial disposition (white dashed line) (sample CÑ105). (J) Scarce and dispersed disarticulated calcitic valves (sample CÑ105). (K) Homogeneous to grumous micrite matrix with peloidal texture (sample CÑ106). (L) Faint fenestral appearance (sample CÑ106). (M) Scarce and dispersed siliciclasts, some replaced by carbonate (corrosion) with bright orange luminescence (sample CÑ106). (N) Homogeneous micritic matrix with dull luminescence. Moderate luminescence microspar cement on the fenestrae. Blocky spar disarticulated valve with weak to no luminescence (white dashed line) (sample CÑ106). (O) Homogeneous and grumous micrite matrix with vertically aligned disruptive structures (birds eye) with microspar margins (sample CÑ108). B.cc., bladed calcite; C, cement; GM, Gromous micrite; I, Intraclast; m, Meniscus cement; Sc, Siliciclast; V, valves.



interparticle connections between adjacent carbonate grains are interpreted as meniscus cement characteristic of the vadose subenvironment (Armenteros, 2010; Christ et al., 2018). However, the presence of granular

calcite cement filling the remaining pores strongly suggests a change to a meteoric-phreatic environment during burial (Flügel, 2010). The bright luminescence of the rims is interpreted as possibly precipitating under low

Fe concentrations and the presence of Mn in an oxygen-poor microenvironment (Hiatt & Pufahl, 2014; Christ et al., 2018). The dull luminescence, dark bladed calcite is interpreted as forming in the phreatic meteoric subenvironment (Flügel, 2010) under high Fe and/or low Mn concentrations (Machel, 2000). The dark brown, dull luminescence granular spar is interpreted as due to the presence of Fe in a reducing microenvironment (Hiatt & Pufahl, 2014).

6.3 | Microfacies: Silty grainstone

6.3.1 | Description

This microfacies has a grain-supported siliciclastic microfabric with abundant carbonate intraclasts of grumous micrite. The intraclasts are subangular to subrounded 240–2000 μm in size, while a few of them contain horizontal crenulated laminations which measure 25 μm in thickness. Some intraclasts are elongated and have different crenulated layers of microspar (Figure 8H), whereas others contain radially disposed straight tubules 25 μm thick and 240 μm long. There are also scarce rounded intraclasts with faint tubules of the same size radially disposed to form structures 300 μm thick (Figure 8I). This radial disposition of tubular structures originates from a structureless micrite differentiated nuclei. The micrite intraclasts contain scarce and dispersed calcitic disarticulated valves, 350 μm long and 12 μm wide (Figure 8J). Abundant angular siliciclastic grains of quartz, feldspar and biotite (240–700 μm) occur randomly dispersed. Some of them have corroded margins. There are devitrified lithoclasts filling voids and vugs and also patches of zebraic chalcedony 350–4500 μm across.

6.3.2 | Interpretation

Sorting and shape of siliciclastic grains suggest a moderate- to high-energy subenvironment and transport from proximal areas. Micritic intraclasts are interpreted as transported by tractive flows from their original subenvironment. Their shape suggests transport distance was minor. Crenulated micrite is commonly the result of microbial biofilms inducing precipitation of carbonate (Dupraz et al., 2009). The tubular structures are interpreted as due to filamentous algae (Freytet & Verrecchia, 1998; Astibia et al., 2012; Benavente et al., 2012). These two features strongly support that the micrite was biogenic and carbonate precipitation was probably biogenically induced (Dupraz et al., 2009). The disarticulated and fragmented valves might belong to ostracods or bivalves

(Cohen, 2003; Gierlowski-Kordesch, 2010). Transported carbonate grains with shell fragments are common in moderate- to high-energy lacustrine ramp margins (Platt & Wright, 1991). The corroded siliciclastic grains probably were transported from distant areas.

6.4 | Microfacies: Disrupted micrite

6.4.1 | Description

This microfacies is composed of grumous micrite (Figure 8K,L) disrupted by abundant circumgranular and straight cracks 120 μm wide and 700 μm long, and microspar patches. The patches are vertically to subhorizontally aligned and more abundant towards the top, measuring between 25 μm and 3500 μm in length. Crystals of the spar infilling the cracks vary between 25 μm and 50 μm in their major axis and form blocky mosaics. There are scarce disarticulated and neomorphosed valves and siliciclastic grains. Valves measure 120 μm long and 12 μm wide and are replaced by granular calcite. Siliciclastic grains are very scarce and dispersed and include angular silt-sized (25–50 μm) grains of quartz. There are also numerous subrounded empty voids 25–50 μm in diameter. Cathodoluminescence shows a dull luminescence matrix (Figure 8M,N). Some clasts are partially replaced by carbonate (corrosion) and show bright orange luminescence (Figure 8M). A moderate luminescence microspar cement is observed in the patches, whereas the blocky calcite in cracks and valves is non-luminescent (Figure 8N).

6.4.2 | Interpretation

Homogeneous micrite precipitated subaqueously and the grumous texture of the carbonate suggests biogenically induced precipitation (Dupraz et al., 2009). The presence of circumgranular cracks and microspar patches represent subaerial exposure of the micrite and decay of the microorganisms that induced carbonate precipitation (Flügel, 2010; Alonso-Zarza & Wright, 2010). These structures form in microbial micrite when part of the biofilm dies after subaerial exposure which also supports that the micrite is biogenic (Alonso-Zarza & Wright, 2010). The valves are interpreted as ostracods and support a subaqueous subenvironment interpretation (Gierlowski-Kordesch, 2010). This carbonate microfacies also records a shallowing-upward history (Figure 6) (Gierlowski-Kordesch et al., 1991; Platt & Wright, 1991). The dull luminescent grumous micrite matrix is interpreted as preserved primary micrite (Benavente et al., 2023). Straight cracks are interpreted as the result of mechanical compaction

(Flügel, 2010). Microspar with moderate luminescence corresponds to dissolution of the original micrite and subsequent cement precipitation (Armenteros, 2010). The non-luminescent blocky spar in cracks is interpreted as diagenesis in the meteoric vadose and/or phreatic zones (Armenteros, 2010; Flügel, 2010). Bright luminescence in corroded clasts resulted from cementation with Mn presence and non-Fe (Hiatt & Pufahl, 2014).

6.5 | Microfacies: Birds eye micrite

6.5.1 | Description

This microfacies consists of grumous micrite matrix with abundant vertically aligned disruptive structures (birds-eye) with microspar margins that measure between 25 µm and 70 µm (Figure 8O). Particles include very scarce angular silt-sized grains of quartz (35 µm), and articulated ostracod valves that form voids (360–470 µm long and 240 µm wide). This microfacies also has aligned patches of black clotted and dark reddish opaque material.

6.5.2 | Interpretation

The grumous micrite is interpreted as biogenic in origin (Dupraz et al., 2009) that precipitates subaqueously (Gierlowski-Kordesch, 2010) whereas birds-eye structures commonly form as a result of subaerial exposure of microbial biofilms, necrosis and gas generation that made the pores in the resulting fabric (Flügel, 2010). This implies that the limestone bed records lake-level fluctuations (Tucker & Wright, 2002). The presence of ostracods supports a subaqueous subenvironment (De Deckker & Forester, 1988; Gierlowski-Kordesch, 2010). The opaque and dark material is interpreted as OM (*sensu* Tucker & Wright, 2002; Scholle & Ulmer-Scholle, 2003).

6.6 | Microfacies: Bioclastic mudstone

6.6.1 | Description

The bioclastic mudstone microfacies has a siliciclastic matrix with abundant dispersed disarticulated sparitic valves of ostracods (240–600 µm long and 25 µm thick). Valves are oriented concave-up or concave-down with the major axis parallel to lamination. Most of the valves are filled or replaced by fibrous calcite cement (Figure 9A), and some disarticulated valves appear to have calcite acicular crystals that range in size from 60 to 175 µm long and are 12 µm wide. The matrix includes abundant and

randomly dispersed angular silt to very fine sized grains of quartz and feldspar (25 and 70 µm in their major axis). Cathodoluminescence shows a non-luminescence fine-grained siliciclastic matrix with moderate luminescence carbonate in bioclasts, overgrowth cement and filling microfractures (Figure 9B,C).

6.6.2 | Interpretation

Concentrations of valves is interpreted as the result of transport from their original subenvironment by tractive flows. The shell alignment observed is indicative of a predominantly low-energy ramp-type lacustrine margin with episodic reworking processes (Platt & Wright, 1991; Tucker & Wright, 2002). The non-luminescent matrix is indicative of an oxidising microenvironment probably devoid of Mn (Tucker & Wright, 2002). Moderate luminescence microfractures, cement and bioclasts can reflect low Fe and moderate Mn concentrations (Scholle & Ulmer-Scholle, 2003). The fibrous spar cement corresponds to the fossilisation process and characterises the meteoric vadose and phreatic zone (Flügel, 2010; Armenteros, 2010). The acicular spar crystals in bioclasts suggest mixed conditions and/or marine zones during fossil diagenesis (Flügel, 2010).

6.7 | Microfacies: Calcimudstone with sparse detrital grains

6.7.1 | Description

This microfacies contains abundant angular silt-size grains of quartz and feldspar (25 and 60 µm), in a grumous micrite matrix disrupted by vertical and horizontal cracks. Particles also include rare disarticulated and randomly oriented ostracod valves that range in size from 350 to 700 µm long and 12–25 µm wide (Figure 9D,E). Cathodoluminescence shows a dull brown to non-luminescent matrix (Figure 9F), as well as non-luminescent siliciclastic grains, which are concentrated on fractures (Figure 9F,G). Fractures show an isopachous calcite, non-luminescent cement rim that measures 50–150 µm thick, possessing dull luminescence in the centre (Figure 9F). The matrix is disrupted by vertical and horizontal cracks that have bright orange luminescence, whereas ostracod valves are non-luminescent (Figure 9H,I).

6.7.2 | Interpretation

Grumous micrite is interpreted as the result of biogenically induced precipitation (Dupraz et al., 2009).

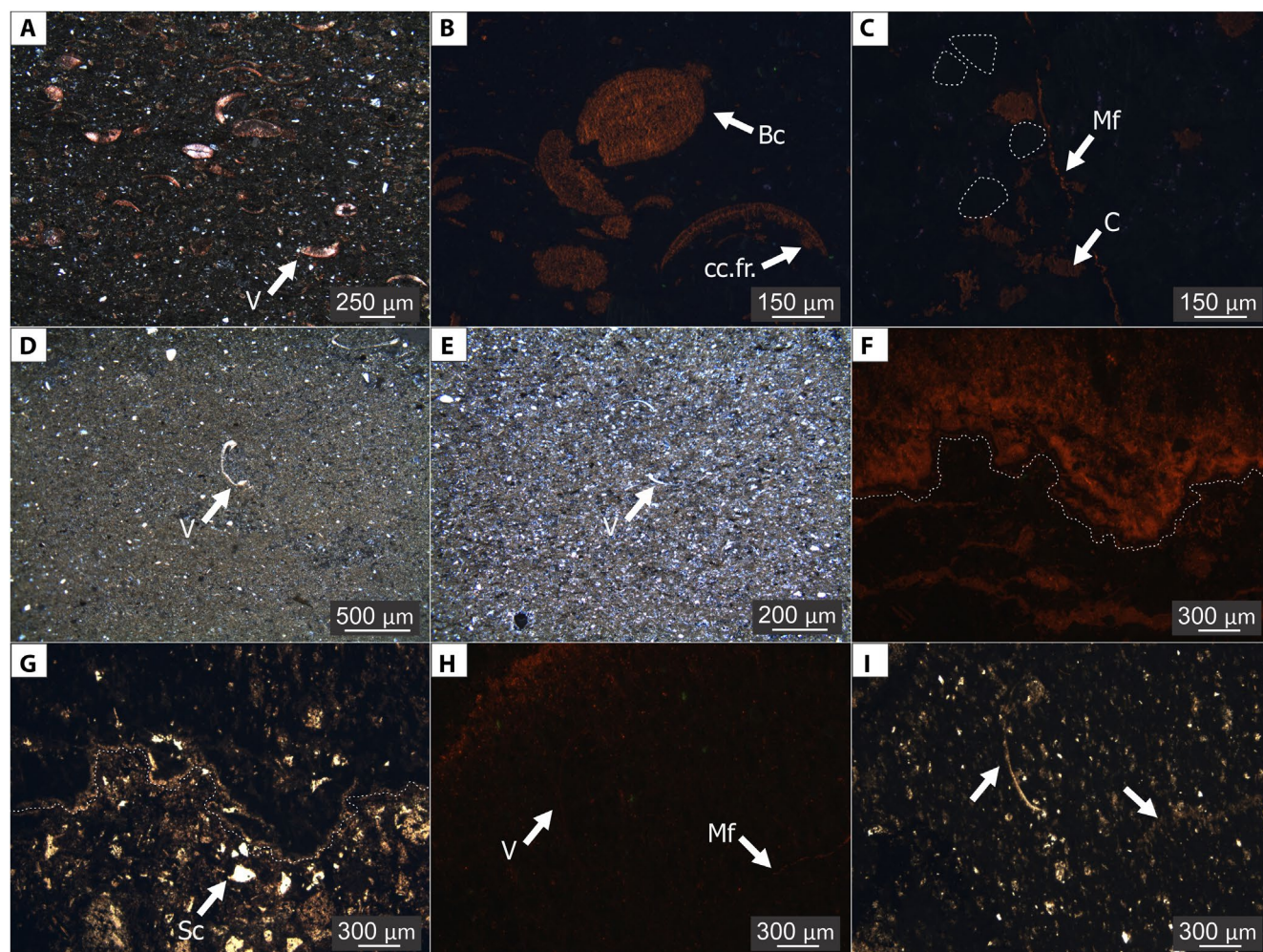


FIGURE 9 Microphotographs of some of the limestone beds sampled in the Ñirihuau Formation middle section at the DAV stratigraphic section. (A) Abundant disarticulated sparitic valves dispersed in the siliciclastic fine-grained matrix (sample DAV4). Some have fibrous spar cement. (B) Fine-grained matrix with very weak to no-luminescence. Abundant dispersed bioclasts with moderate luminescence. Some disarticulated valves present calcite fibroradial overgrowth (sample DAV4). (C) Bright luminescence microfractures affecting the non-luminescent matrix (sample DAV4). The white-dashed lines indicate some of the angular non-luminescent siliciclasts dispersed in the matrix. (D) Grumous micrite matrix with very abundant angular siliciclastic grains of quartz and feldspar and rare disarticulated sparitic valves (sample DAV17). (E) Abundant randomly oriented valves dispersed in a micritic matrix (sample DAV16). (F) A dull brown to non-luminescent matrix disrupted by fractures filled with non-luminescent siliciclasts (sample DAV17). The white dashed line indicates the isopachous spar rim filling fractures with no-luminescence near their margins and dull luminescence in their centre. (G) Same picture as Figure 9F but under parallel polarised light. The siliciclasts can be distinguished. (H) Scarce disarticulated valves dispersed in the grumous micrite matrix (both dull to non-luminescent) (sample DAV17). Some thin microfractures affect the matrix with bright orange luminescence. (I) Same picture as Figure 9H but under parallel polarised light. The arrows indicate the position of the valve and microfracture on Figure 9H. Bc, bioclasts; C, cement; cc. fr. calcite fibroradial overgrowth; Mf, microfracture; Sc, siliciclasts.; V, valves.

Valves are most likely from bivalves (Gierlowski-Kordesch, 2010). This accords with previous descriptions where bivalves of *Diplodon* sp. genus (Unionoida) were reported from the unit (Santonja et al., 2021). The abundance of angular siliciclastic grains and the scarce valves suggest a high-energy setting (Platt & Wright, 1991) very close to the clastic supply area. The dull brown luminescence to non-luminescence of the matrix is interpreted as the result of low Mn and the presence of Fe in a reducing microenvironment (Hiatt & Pufahl, 2014). Similarly, the

non-luminescent spar rim in fracture margins and dull luminescence in their centre correspond to low Mn concentrations and the presence of Fe (Hiatt & Pufahl, 2014). The bright orange luminescence of the cracks is interpreted as the opposite situation (Richter et al., 2003). Non-luminescent valves are interpreted as high Fe concentrations and/or Mn absence (Machel, 2000). Although the sample lacks diagnostic features to constrain the diagenetic zone, based on the observed cements, meteoric conditions can be interpreted.

6.8 | Microfacies: Fenestral micrite

6.8.1 | Description

This microfacies is dominated by grumous micrite with rare siliciclastic grains of quartz and feldspar (Figure 10A) that measure 120–290 μm in diameter; and scarce disarticulated valves that measure 240–350 μm long and 12–25 μm

wide. The matrix is characterised by abundant irregularly distributed LF-BI type fenestrae that measure between 200 μm and 500 μm across. Some of the fenestral space has been filled by microcrystalline quartz (Figure 10A,B). The micrite and patches of blocky spar cement show bright orange luminescence (Figure 10C). The valves and siliciclastic grains have dark brown dull luminescence or are non-luminescent (Figure 10C).

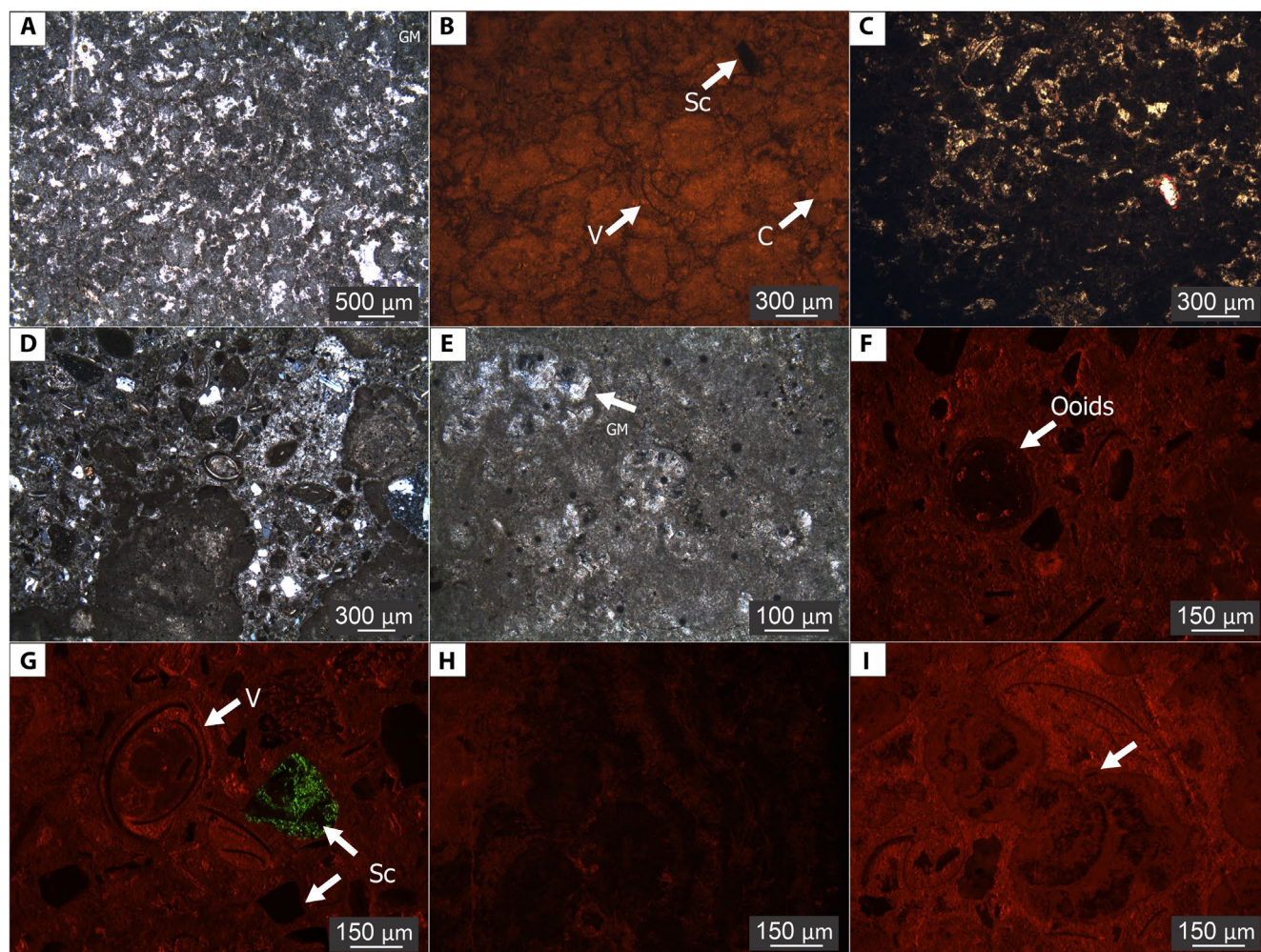


FIGURE 10 Microphotographs of the limestone beds sampled in the Ñirihuau Formation at Cerro Carbón and Arroyo del Medio sites. (A) Grumous micrite with rare siliciclastic grains of quartz and feldspar and scarce disarticulated valves. Some of the fenestral space has been filled by microcrystalline quartz (sample CAR18). (B) Grumous micrite matrix is observed with bright orange luminescent matrix. Scarce siliciclasts and disarticulated valves with dark brown dull luminescence or non-luminescence are dispersed in the matrix (sample CAR18). (C) Same picture as (B) but under parallel polarised light. The red dashed line indicates the position of the clast marked in (B). (D) Grumous micrite matrix disrupted by cracks filled by inequigranular mosaics of spar, angular siliciclasts and disarticulated sparitic valves (sample AME1). Valves can have a concentric black dark opaque material coating. (E) White arrow points to the aggrading fibro-radial spar structures dispersed in the grumous micrite matrix observed (sample AME1). They overlap up to three layers. (F) Mottled micrite with high orange luminescence (sample AME1). Bioclasts, ooids, clasts and other particles of dull luminescence with a cement of bright luminescence filling the voids are observed. (G) Fitted disarticulated valves and other particles of dull luminescence with a cement of bright luminescence filling the voids (sample AME1). (H) Interlayered thin laminae of fibro-radial spar forms alternating dull and non-luminescent layers indicative of a possible biogenic origin (sample AME1). (I) Thin laminae of fibro-radial spar interlayered with alternate brighter and weaker luminescence of possible biogenic origin (sample AME1). C, cement; GM, Grumous micrite.; Sc, siliciclasts; V, valves.

6.8.2 | Interpretation

Grumous micrite is interpreted as the result of biogenically induced precipitation (Dupraz et al., 2009). Fenestrae are commonly formed when microbial mats or biofilms are subaerially exposed (Flügel, 2010), this suggests that the carbonate precipitated subaqueously and was subsequently exposed (Alonso-Zarza & Wright, 2010). Blocky spar characterises the meteoric vadose and/or phreatic diagenetic zones (Armenteros, 2010). Bright orange luminescent micrite and spar cement are interpreted as due to a high concentration of Mn and a low concentration of Fe in an oxygen-poor microenvironment (Hiatt & Pufahl, 2014).

6.9 | Microfacies: Stromatolitic boundstone

6.9.1 | Description

This microfacies has a matrix of grumous micrite disrupted with cracks filled by inequigranular mosaics of spar, angular siliciclasts and disarticulated sparitic valves (Figure 10D,E). The spar crystals measure between 40 µm and 200 µm along their major axis. The valves are 200–800 µm in length and 20 µm thick. They can have a concentric coating of a dark black opaque material 30 µm thick (Figure 10D). The margins of the cracks are smooth with dense micrite or concentrations of opaque material and dark pellets 20 µm in diameter. Dispersed in the matrix are aggrading fibrous spar structures that overlap up to three layers of fibro-radial spar, where the crystals have their long axis perpendicular to the micrite lamination. At their greatest extent, these structures measure up to 30 µm long and 100 µm wide but they are narrower at their base (Figure 10E), with lateral changes to micrite. There are dispersed aggregate carbonate grains that range in size from 100 to 300 µm in diameter (Figure 10F,G). There are also voids and interparticle spaces dispersed in the matrix that have been filled with spar mosaics and present a 10 µm thick circumgranular spar rim. Mottled micrite and spar carbonate cement have bright orange luminescence. The fibro-radial spar forms alternating dull and non-luminescent layers (Figure 10H,I). Valves have dark orange low luminescence. Feldspar crystals are fractured and their fractures are filled with a bright luminescent carbonate cement. Microstylolites are non-luminescent.

6.9.2 | Interpretation

The grumous micrite microfabric is indicative of biogenically induced carbonate precipitation (Chafetz &

Buczynski, 1992; Dupraz et al., 2009), and not trapping and binding (Burne & Moore, 1987) as would have been expected from the macrofabric (Braga et al., 1995). Fibro-radial sparitic aggrading structures are interpreted as biogenic build up structures and are the microscopic expression of the domal stromatolitic macrofabric observed in outcrop. Sparitic valves are interpreted as ostracods (Gierlowski-Kordesch, 2010). Their inclusion in coated structures forming incipient carbonate aggregate grains indicates agitation in a high-energy environment (Arenas et al., 2007). Micritic fragments observed in the aggregates are interpreted as originating from fragmentation of biogenic structures in a moderate- to high-energy environment and coated by agitation of the water column (Flügel, 2010). Fibro-radial spar is typical of the meteoric vadose diagenetic zone (Flügel, 2010). The circumgranular rim and corroding cement in the siliciclasts with bright orange luminescence are interpreted as forming in the meteoric phreatic zone with low Fe concentrations and the presence of Mn (Flügel, 2010; Hiatt & Pufahl, 2014). The fibro-radial spar with alternating dull and non-luminescent layers could be a response to variations in the OM content between layers, which in turn, exhibit a different response to diagenesis (Icole et al., 1990). Dark orange, dull luminescent sparitic bioclasts are interpreted as the result of cementation in an oxidising microenvironment (Hiatt & Pufahl, 2014).

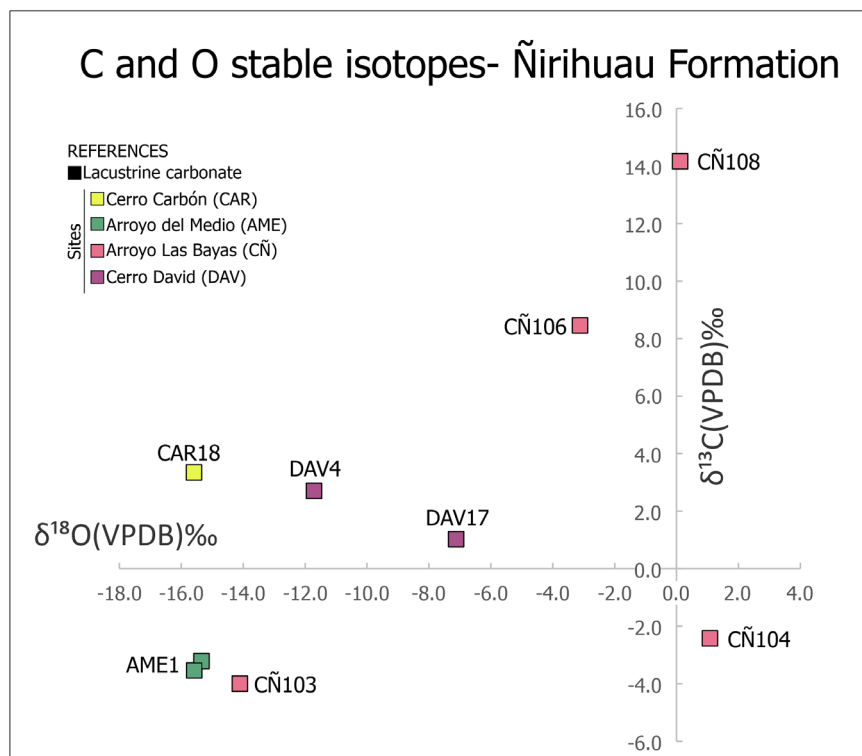
7 | CARBON AND OXYGEN STABLE ISOTOPE COMPOSITION

The limestone samples analysed from the Ñirihuau Formation at the Cerro Carbón (CAR), Arroyo del Medio (AME), Arroyo Las Bayas (CÑ) and Cerro David (DAV) sites (Figure 2; Table 3) have $\delta^{18}\text{O}_{\text{cal}}$ values that range between +1.1 and −15.6‰ (χ average = −9.0‰; 1σ = 7.8; N = 9) and $\delta^{13}\text{C}_{\text{cal}}$ values that range from +14.2 to −4.0‰ (χ average = 1.8‰; 1σ = 6.2; N = 9) (Table 3; Figure 11). These are broad ranges for both the O and C isotope values. The correlation coefficient between $\delta^{18}\text{O}_{\text{cal}}$ and $\delta^{13}\text{C}_{\text{cal}}$ is $r = 0.56$ ($r < 0.7$), $p = 0.15$, indicating a low correlation between the variables tested; however, the number of samples analysed is small ($n = 9$).

7.1 | Interpretation

The $\delta^{13}\text{C}_{\text{cal}}$ values obtained range from positive to negative values, but most of them are positive (Figure 11). This is consistent with several different processes such as accumulation of OM at the bottom of a stratified lake system, fractionation due to exchange with atmospheric

FIGURE 11 Cross-plot of $\delta^{18}\text{O}$ and $\delta^{13}\text{C}$ data for the Ñirihuau Formation carbonates, comparing the values from Arroyo Las Bayas and Cerro David, located at the western and eastern flanks of the David Syncline, and from the Cerro Carbón and Arroyo del Medio localities. Note that there are two points from Arroyo del Medio that correspond to carbon and oxygen stable isotope analysis conducted on two different samples from the same carbonate bed. VPDB, Vienna Pee Dee belemnite standard.



CO_2 , or a limestone-rich catchment (Leng et al., 2005). The latter can be dismissed as there is no record of older carbonates in the study area. Extremely positive values like the one from sample CÑ108 have been attributed to methanogenic bacteria in the lake waters (Potter et al., 2004). However, there is not a well-defined trend in the data set to infer that effect for carbonate precipitation. Nevertheless, the $\delta^{13}\text{C}_{\text{cal}}$ values obtained for the CÑ site show a stratigraphic trend from more negative to positive values, which could indicate the effect of exchange with atmospheric CO_2 through time, or perhaps volcanic influence. A volcanic effect has been interpreted in modern lakes (Valero-Garcés et al., 1999) and could be a more plausible interpretation for the more positive $\delta^{13}\text{C}_{\text{cal}}$ values of the Ñirihuau Formation since significant pyroclastic material is recorded interfingered in the lacustrine sedimentary succession that contains the carbonates (Santonja et al., 2021). Alternatively, negative values might be linked to the mixing of waters during the seasonal breakdown of lake water stratification and the decomposition of OM (Leng & Marshall, 2004). This stratification is inferred based on the sedimentary features observed in the lacustrine deposits of the Ñirihuau Formation middle section, such as the dark-coloured laminated mudstones (Fl) found in the lake-centre facies (Santonja et al., 2021), where the calm and less oxygenated deep-water area favoured the settling of fine material (Håkanson, 2007), that contrast with Facies 1 and 2 (Marginal lacustrine

and Lower-delta plain facies, respectively), where there is evidence of agitation of the lake surface by waves and circulation, generating an oxygenated environment (Nichols, 2009).

The $\delta^{18}\text{O}_{\text{cal}}$ values obtained range from positive to negative but most of them are negative, reaching values of -15.6‰ . This is consistent with meteoric water origins and possibly groundwater supply (Leng et al., 2005). Positive values might reflect an evaporative effect operating in the lacustrine system, whereas negative values represent dilution stages with significant water input (Leng et al., 2005). This accords with the microfacies where the positive values are recorded (birds eye micrite and homogeneous calcimudstone), since both present evidence of subaerial exposure. The $\delta^{18}\text{O}$ values obtained for the Arroyo las Bayas site (CÑ samples) show alternating negative and positive values that could potentially indicate repeating diluted and evaporative stages (lake-level fluctuations). However, the small number of samples demands caution in the interpretation.

The low correlation coefficient ($r < 0.7$) between carbon and oxygen isotope data points to a short residence time for the palaeolake waters, which would indicate an open hydrology for the system (Talbot, 1990; Leng et al., 2005; Alonso-Zarza et al., 2012). However, while the data set presents scattered data points representing four different sites across the palaeolake, it lacks the high temporal resolution required to allow such an interpretation for the lacustrine system.

8 | DISCUSSION

8.1 | Lacustrine depositional environment

According to the sedimentological evidence from the four sites analysed, a littoral lacustrine environment can be identified (Platt & Wright, 1991). In the stratigraphic sections studied, carbonate production is recognised in the marginal lacustrine (Facies 1), and lower delta-plain (Facies 2) facies. Nearshore carbonate production is mostly biogenic or bio-induced although inorganic carbonate precipitation may also occur in shallow water (Platt & Wright, 1991). According to previous provenance analysis conducted by Santonja et al. (2021), this lacustrine system of the middle Ñirihuau Formation contains a substantial amount of volcanoclastic material of intermediate to basic composition, which most likely came from the erosion of the El Maitén Volcanic Belt (Figure 1; Rapela et al., 1988; Fernández Paz et al., 2019), or by effusions synchronous with sedimentation, linked to the contemporaneous magmatic arc. At that time, the main sediment sources would have been located to the west of the basin.

The Ñirihuau carbonate microfacies and facies accumulated under both low- and high-energy conditions (Platt & Wright, 1991). High- to moderate-energy microfacies and facies have been recognised mainly at CAR (in the north) and DAV (in the south), with the development of carbonate deposits accumulated by tractive flows such as bioclast concentrations and sedimentary structures, such as GRm, GRt and GRh, which are also observed in the clastic deposits (Sr, Srw, Sh, Sl, St). Moderate- to low-energy carbonate sedimentation is identified at AME, represented by stromatolite aggradation. The development of the laterally connected domal carbonate structures could be favoured by physical barriers, such as sand bars, that protect them from high-energy currents. The low-energy carbonate precipitation is characterised by micritic and intraclastic carbonate microfacies, and can present evidence of subaerial exposure (Tucker & Wright, 2002). Those features have been found principally at CÑ, represented mainly by biogenically induced micrite precipitation and by the absence of sedimentary structures that indicate high-energy processes. The desiccation cracks found in sample CÑ104 (Homogeneous calcimudstone), which are superimposed on carbonates with subaqueous features, could indicate that lake-level fluctuations were rapid. Subaerial exposure is also supported by birds eye micrite structures from sample CÑ108. This supports the hypothesis that this margin of the lake system had a low gradient, where minor lake-level fluctuations could have led to significant surface exposure.

In light of the aforementioned features and according to the distribution and characteristics of the different sites analysed, it could be argued that the palaeolake system had a variable physiographic configuration (Figure 12). However, the variations observed in the different sectors of the basin are not necessarily only spatial variations within the lacustrine system. There may also be temporal differences because limestones are present in both the first and the second lacustrine systems of the middle Ñirihuau Formation (Santonja et al., 2021), but further stratigraphic correlations are necessary to determine this.

The Ñirihuau palaeolake could correspond to either the fluctuating-profundal or the fluvial-lacustrine facies associations that characterise balanced-fill and overfilled lake basin types, respectively (*sensu* Bohacs et al., 2000). This conclusion is based on the detailed stratigraphic analysis of the middle Ñirihuau Formation, sedimentary structures observed, abundant freshwater fossils (Bocchino, 1964; Aragón & Romero, 1984; Pascual et al., 1984; Cazau et al., 1989; Aguirre-Urreta, 1992; Bertels-Potka & Cusminsky, 1999; Cione & Báez, 2007; Santonja et al., 2021; this contribution), and the progradational stratal stacking patterns which demonstrate mixtures of the characteristics of the two lacustrine facies associations.

A balanced-fill lake basin (Bohacs et al., 2000) occurs when the rates of sediment plus water supply relative to potential accommodation, are relatively equal over the time span of sequence development. Periodically, water inflows are sufficient to fill available accommodation, but are not always matched by outflow. Consequently, lake-level fluctuations driven by climate are common. This lake-basin type generally records a combination of progradation of clastic sediments and vertical aggradation of chemical sediments due to desiccation cycles. On the other hand, an overfilled lake (Bohacs et al., 2000), occurs when the rate of supply of sediment and water consistently exceeds potential accommodation and where water inflows are in equilibrium with outflows. These types of lakes are very closely related to perennial river systems. Their deposits are commonly interbedded with fluvial deposits and coals (fluvial-lacustrine facies associations). Carbonates are generally abundant in both types of lakes but differ in their detailed characteristics. However, the features identified were inconclusive for either type of lake basin. Therefore, with the observations presented here, no major distinction could be made between balanced-fill and overfilled lake basins. Further sedimentary analyses and correlation of more stratigraphic successions need to be made, concentrating on the relationships between various facies and carbonate types in vertical and lateral sequences, their stacking patterns, and the detailed characteristics

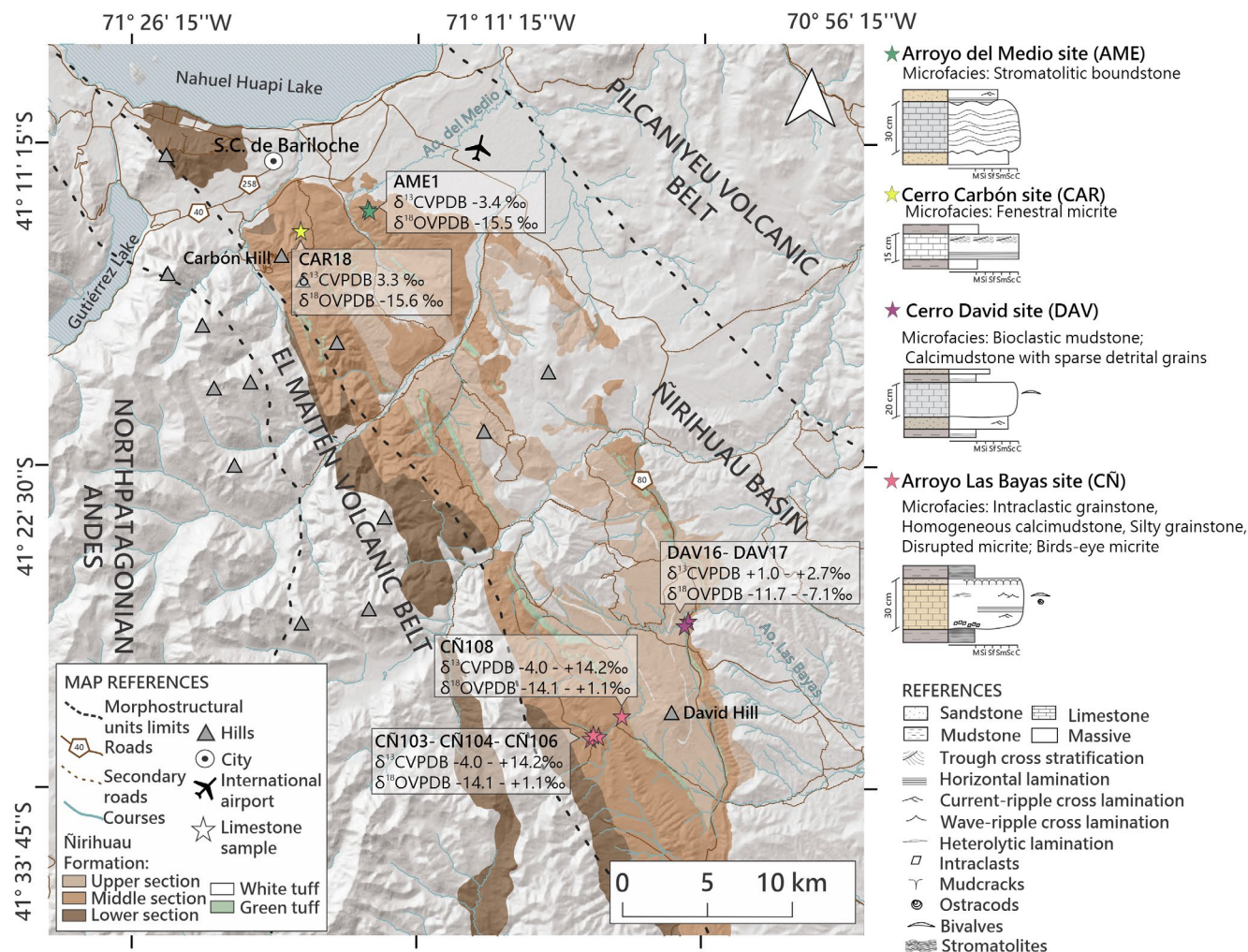


FIGURE 12 Regional map showing the morpho-structural units, the Ñirihuau Formation outcrops and the location of the limestone beds sampled along the northernmost sector of the Ñirihuau Basin (See Figure 1 for location and further references). Each star represents a single sample. The stable isotope analysis results ($\delta^{18}\text{O}$ and $\delta^{13}\text{C}$ minimum and maximum values) are shown in the picture next to the corresponding samples for each site. At Arroyo del Medio (green star), an average of the results of the two samples analysed from the same bed is shown. Schematic logs of the limestone bed outcrops from the different sites are represented with their main macroscopic and microscopic characteristics synthesised. The colour of the lithologic column represents the colour of the deposit.

of OM, in order to proceed with the classification and determine the lake basin type for the middle section of the Ñirihuau Formation.

8.2 | Carbonate diagenesis

Petrographic and cathodoluminescence analyses reveal different diagenetic phases which affect the primary fabric of the carbonate in the Ñirihuau Formation. The diagenetic phases were identified following the proposal of Armenteros (2010).

The grumous to homogeneous micrite observed in some samples (Table 3; Figures 8D through G, K through O, 9D through I and 10) is considered to be primary precipitated calcite (Murphy Jr. et al., 2014), suggesting

biogenically induced precipitation of carbonate (Dupraz et al., 2009; Taher & Abdel-Motelib, 2014). Therefore, this micrite records the primary conditions of carbonate precipitation in continental palaeoenvironments through its stable-isotope composition.

Valves recognised in all microfacies are mainly sparitic and they preserve their original morphology very well, pointing to a meteoric-vadose diagenetic zone during fossil diagenesis (Armenteros, 2010). Sparitic and microsparitic cements, identified in all the microfacies, are restricted to cracks, voids and rims. Their habit and luminescence are highly variable, pointing to different stages and diagenetic zones (Armenteros, 2010). Petrographic features of the different cements have allowed the identification of a meteoric-diagenetic zone, ranging from vadose to phreatic (Flügel, 2010; Armenteros, 2010) (Table 3). There is

an exception for the Bioclastic mudstone microfacies from the Cerro David site (DAV). This microfacies shows a fibrous spar cement, characterising the meteoric-vadose diagenetic zone (Flügel, 2010; Armenteros, 2010), but also some of the bioclasts in it appear to present acicular spar overgrowth (Table 3; Figure 10F through I). This cement has been reported either for the mixed meteoric-marine diagenetic zone or the marine diagenetic zone (Tucker & Wright, 2002; Flügel, 2010). In the case of the Ñirihuau Formation, it has been proposed that deposition occurred mainly in continental fluvial and lacustrine environments, but also with a restricted marine incursion. The marine interpretation is based on the occurrence of marine microfossils (dinoflagellates and acritarchs), marine molluscs, heterolithic sedimentary structures and mud drapes and bedding patterns found in the northern sector of the basin (Spalletti, 1981, 1983; Asensio et al., 2004; Cazau et al., 1989; González Bonorino & González Bonorino, 1978; Ramos, 1982). In this context, the acicular spar cement involved in fossil diagenesis could be considered an indicator of a mixed meteoric/marine diagenetic zone in the eastern margin of the basin. However, additional data is needed to confirm this interpretation.

Cathodoluminescence shows that the micrite is characterised by low to no luminescence in most of the samples, reinforcing the petrographic interpretation of it as a primary feature. Two samples from the north of the basin, however, a stromatolitic boundstone from the Arroyo del Medio site and a fenestral micrite from the Cerro Carbón site, exhibit bright luminescence of the grumous or homogeneous micritic matrix (Table 3; Figure 10). This would indicate a very early stage of diagenesis (eogenesis), possibly simultaneous with primary carbonate precipitation, implying that the north area of the basin had substantial pore-fluid influx at a very early stage during carbonate precipitation.

The various spar cements found, being fibrous, bladed, granular, blocky and isopachous, have mostly weak to moderate luminescence. Only cracks filled with spar in one sample (calcimudstone with sparse detrital grains microfacies from DAV) show bright luminescence (Figure 9F,H). This again points to the southern area as a distinct sector, in this case with a different composition of the fluids involved in the diagenesis of the deposit. Only one sample from AME, in the north (Figure 12), presents evidence for chemical compaction as microstylolites. The lack of this kind of structure in most of the samples suggests that deep burial diagenesis (mesogenesis) was minor in this area of the basin (Bathurst, 1975; Choquette & James, 1987).

The combination of petrographic features and their response under cathodoluminescence indicates a predominance of mineral precipitation in the meteoric-vadose and

meteoric-phreatic zones, with variations in the redox conditions. This supports the interpretation of an eogenetic to a shallow mesogenetic diagenetic stage (Bathurst, 1975; Table 3).

8.3 | Palaeoclimate inferences

Oxygen and carbon stable-isotope records have served as the principal means of reconstructing global and regional climate change on a variety of geologic time-scales (Emiliani & Edwards, 1953; Savin et al., 1975; Shackleton, 1987; Matthews & Poore, 1981; Miller & Katz, 1987; Zachos et al., 2001). Also, lakes serve as highly sensitive and dynamic systems with the potential to record climate changes, such as shifts in precipitation patterns (Tucker & Wright, 1990; Leng & Marshall, 2004; Gierlowski-Kordesch, 2010). Lacustrine carbonates are particularly useful for tracking this information and hence represent a valuable palaeoenvironmental record (Lüdecke et al., 2013).

Lake waters are part of the meteoric water cycle and the oxygen isotopic composition of meteoric waters ($\delta^{18}\text{O}_{\text{mw}}$) is affected by many factors. The most important fractionation mechanisms for water are evaporation and condensation at the hydrosphere-atmosphere interface (Horita & Wesolowski, 1994). The $\delta^{18}\text{O}$ composition of lake water ($\delta^{18}\text{O}_{\text{lw}}$) is influenced by the oxygen isotopic composition of meteoric waters supplied to the lake, by precipitation, surface run-off and groundwater inflow. Evaporation, itself governed by temperature and relative humidity, strongly controls depletion of the light oxygen isotope ^{16}O in the liquid-water phase. Changes in temperature, rainfall sources, riverine influx and groundwater input are recorded in the oxygen isotope ratios of carbonates ($\delta^{18}\text{O}_{\text{carb}}$) which precipitate from lake water (Turner et al., 1983; Talbot, 1990; Teranes et al., 1999; Lamb et al., 2000; Schwalb & Dean, 2002; Leng & Marshall, 2004; Yansa et al., 2007; Davis et al., 2009; Deocampo, 2010; Kent-Corson et al., 2010). Stratigraphic changes in $\delta^{18}\text{O}_{\text{carb}}$ values of lacustrine sections can therefore be attributed to changes in $\delta^{18}\text{O}_{\text{lw}}$ or temperature (Leng & Marshall, 2004; Leng et al., 2005).

$\delta^{13}\text{C}$ values in lacustrine environments are controlled by three main processes: (1) $\delta^{13}\text{C}$ composition of inflowing waters, (2) CO_2 exchange between atmosphere and the total dissolved inorganic carbon (TDIC) and (3) photosynthesis/respiration of aquatic plants and algae within the lake (Leng & Marshall, 2004; Leng et al., 2005). In turn, the TDIC concentration in the lacustrine environment is governed by changes in carbon and nutrient cycling, as well as productivity within the lake and its catchment, which are often climatically controlled (Leng & Marshall, 2004; Leng et al., 2005).

The limestone samples analysed from the Ñirihuau Formation at the CAR, AME, CÑ and DAV sites have a broad range of values of $\delta^{18}\text{O}_{\text{carb}}$ (+1.1 to -15.6‰) and $\delta^{13}\text{C}_{\text{carb}}$ (+14.2 to -4.0‰) (Table 3; Figure 11). The $\delta^{18}\text{O}$ lacustrine signature of limestones from DAV presents an alternation of more negative and positive values that suggests possible alternating dilution (more negative values) and evaporation stages (less negative values). Such changes are usually controlled by climate effects but can also be triggered by tectonism modifying drainage networks and/or the catchment area leading to lake-level fluctuations. Therefore, it is difficult to confirm a climate effect on the $\delta^{18}\text{O}$ signature with data this limited.

The $\delta^{18}\text{O}$ values obtained for the Ñirihuau limestone beds agree with the general depletion in $\delta^{18}\text{O}$ values recorded in the global deep-sea curve from Zachos et al. (2001, 2008) during the MMCO, and the $\delta^{13}\text{C}$ data match the range in values of Zachos et al. (2001, 2008) for the same event. During the late Oligocene (26–27 Ma), a warming trend took place, and it lasted until the Middle Miocene (15 Ma). During this period of time, Antarctic ice reduced its extent and global ice volumes remained (relatively) low. With the exception of several brief periods of glaciation, oceanic bottom-water temperatures slightly increased over time (Wright et al., 1992). This warm phase reached its peak from 17 until 15 Ma, during the MMCO (Flower & Kennett, 1994; Hinojosa, 2005; Hinojosa & Villagrán, 2005). Numerical simulations indicate global mean annual temperatures were about 3°C higher than today (You et al., 2009; Knorr et al., 2011). The limestone beds of the Arroyo Las Bayas section (CÑ site), which belong to the first lacustrine system in the Ñirihuau Formation, were deposited during this warm period (Figure 3), according to U–Pb geochronological data published by Santonja et al. (2021). The MMCO was followed by a long-term gradual cooling and re-establishment of a significant ice-sheet on Antarctica by 10 Ma (Zachos et al., 2001). The important process of global climate reorganisation that followed the MMCO is known as the MMCT and took place between *ca* 14.5 and 13 Ma (Flower & Kennett, 1994; Super et al., 2018; Leutert et al., 2021 and references therein). During this period, the deposition of the second lacustrine interval of the Ñirihuau Formation took place (Figure 3A), according to U–Pb dating (Santonja et al., 2021), where sample CÑ108 from the Arroyo las Bayas site (CÑ) and possibly the limestones of the Cerro David site (DAV) were obtained.

According to the vegetation found in Patagonia during the Oligocene and Miocene, the forests were dominated by a cool temperate biome constituted mainly by *Nothofagus* (Barreda & Palazzesi, 2007; Iglesias, et al. 2011; Passalía et al. 2016). However, the short climatic optimum of the Middle Miocene, with

high global temperatures (Zachos et al., 2001), is associated with a marine transgression over Patagonia (Uliana & Biddle, 1988; Barreda et al., 2007; Malumíán & Náñez, 2011) and caused the southward shift of some wet-tropical palaeofloral elements such as *Sapindaceae-Cupania*, Euphorbiaceae, Bombacaceae, Malpighiaceae, Cyperaceae, Sparganiaceae/Tifaceae, Restionaceae, Malvaceae and Polygonaceae (Barreda et al., 2007; Iglesias et al., 2011). Also, pollen records from late Oligocene–Middle Miocene marine strata of Patagonia indicate humid forest conditions dominated by *Nothofagus* and podocarps, with low abundances of arid-adapted (inferred as open habitat) taxa before 10 Ma (Palazzesi & Barreda, 2012; Dunn et al., 2015). Regarding vertebrates, in the Early and Middle Miocene, amphibian calyptocephalleids are recorded in extra-Andean regions of Patagonia, reaching the southernmost tip of the continent, alongside the presence of *Ceratophrys* genus (Fabrezi, 2006; Frost et al., 2006), which extends beyond the southern distribution limit of the calyptocephalleids (*ca* 39°S). This convergence of elements of different biogeographic origin is possibly a result of the warm climate conditions that peaked in the late Middle Miocene (Zachos et al., 2001). The last (youngest) records of calyptocephalleids in Argentina are from the Late Miocene (Cione & Báez, 2007).

A cool temperate to warm temperate and humid climate with a relatively abundant to moderate rainfall regime and the development of bi-seasonality (a cold and a warm season, and a dry and rainy season during the year) has been interpreted from deposits of the lower and middle section of the Ñirihuau Formation, based on megafloora, microflora and fungal evidence (Falaschi et al., 2012; Caviglia & Zamaloa, 2014; Caviglia, 2018; Machado et al., 2022, 2024). These conditions would have lasted until the deposition of the middle section, where the lacustrine carbonates were observed, since a change is recorded later, in the palaeoflora records of the upper section of the Ñirihuau Formation (Passalía et al., 2019) dated with U–Pb between *ca* 13 and 11 Ma (Santonja et al., 2021).

Given all the above-mentioned, the lacustrine carbonates of the middle Ñirihuau Formation were precipitated and accumulated under the temperate to warm and wet conditions that prevailed in Patagonia during the MMCO and the MMCT. These conditions continued until the early stages of the Andean uplift (Middle to Late Miocene; Ramos et al., 2015; Butler et al., 2020; García Morabito et al., 2021; Santonja et al., 2021), whose effects are interpreted to be recorded in the upper Ñirihuau Formation on sedimentary and palaeoenvironmental evidence (Santonja et al., 2021). The orogenic shadow effect of the Patagonian Andes developed after 14.6 Ma (Bucher et al., 2020) would have led to an aridification, due to the

flux of the westerlies discharging water on the western side of the Cordillera leaving dry air circulation to the east (Compagnucci, 2011; Le Roux, 2012). This would have led to the retreat of the flora taxa as a consequence of the lower rainfall regime and dryer conditions on the eastern slope of the Andes (Barreda & Palazzesi, 2021), and to the extinction of several vertebrate lineages (Ortiz-Jaureguizar & Cladera, 2006).

9 | CONCLUSIONS

The precipitation and accumulation of the continental limestone beds in the Ñirihuau Formation in the Ñirihuau Basin occurred in a Ca-rich littoral lacustrine setting, with Facies 1 representing a lake margin and Facies 2 a lower delta plain palaeoenvironment. This lacustrine margin carbonate factory is characterised by abiotic and biotic elements and processes. It was dominated by bio-induced subaqueous carbonate precipitation as well as deposition by tractive flows, and was later affected by subaerial exposure and diagenetic processes.

The main diagenetic zones were the meteoric-vadose and meteoric-phreatic, and the dominant diagenetic stage was eogenesis, associated with scarce signs of chemical compaction that point to shallow mesogenesis processes, according to petrographic and cathodoluminescence analyses. Grumous micrite is interpreted as primary.

Although the low correlation coefficient between $\delta^{13}\text{C}$ and $\delta^{18}\text{O}$ values indicates a short residence time of the palaeolake waters, the lake basin type and its palaeohydrology cannot be adequately defined with the sparse data set presented here. Further sedimentary analyses of more stratigraphic successions within the basin need to be performed to determine those aspects of the lacustrine system that prevailed during deposition of the middle section of the Ñirihuau Formation.

Finally, the $\delta^{18}\text{O}$ and $\delta^{13}\text{C}$ values are consistent with the general values recorded in the global deep sea curve from Zachos et al. (2001, 2008) during the MMCO (17–15 Ma), when most of the limestone beds of the lacustrine system of the middle section of the Ñirihuau Formation were deposited, according to previously published U–Pb data. At that time, temperate to warm seasonal palaeoclimate conditions are interpreted to have prevailed during deposition of these carbonate facies, based on oxygen and carbon stable isotope data together with other proxies, such as fossil flora found in this unit. The outcomes outlined in this study offer a new approach to the current understanding of the past hydrological, depositional and climate conditions that prevailed during the deposition of the lacustrine intervals of the middle section of the Ñirihuau Formation between 15 and 13 Ma.

ACKNOWLEDGEMENTS

This research was funded by Agencia Nacional de Promoción Científica y Tecnológica (PICT-2017-3259, PICT-2018-2356 and PICT 2020-2619 projects) and Universidad Nacional de Río Negro (40-B-743 project). We wish to thank the geologist Zuriñe Larena Martin for her great help and insights during the research short-stay at the Luminescence Laboratory of the Department of Geology at UNS (Universidad Nacional del Sur), where cathodoluminescence analysis was conducted. Also, special thanks to Susana Alonso and Roberto Asta, who prepared the thin sections, for their availability, kindness and the enriching exchanges generated during our meetings. We would like to express our gratitude to Drs. Maisa Tunik and Gabriela Cuminsky for their generous availability and the insightful exchange. Finally, we are deeply grateful to the reviewers Drs. Concha Arenas Abad and Giovanna Della Porta, as well as to the Editor-in-Chief, Peter Swart, and the Associate Editor, Kevin Bohacs, for their criticism and suggestions, which considerably contributed to improving the quality of this manuscript.

CONFLICT OF INTEREST STATEMENT

The authors have no conflict of interest.

DATA AVAILABILITY STATEMENT

Data sharing is not applicable to this article as no data sets were generated or analysed during the current study.

ORCID

Camila Santonja  <https://orcid.org/0000-0003-2815-4979>

Cecilia A. Benavente  <https://orcid.org/0000-0002-3414-0330>

REFERENCES

- Aguirre-Urreta, M.B. (1992) Tertiary freshwater decapada (Crustacea: Parastacidae) from the Ñirihuau basin, Patagonia, Argentina. *Journal of Paleontology*, 66(5), 817–825. <https://doi.org/10.1017/S0022336000020825>
- Alonso-Zarza, A.M. & Tanner, L.H. (2010) Carbonates in continental settings: facies, environments and processes. In: *Developments in sedimentology*, Vol. 61. Amsterdam: Elsevier, p. 307.
- Alonso-Zarza, A.M. & Wright, V.P. (2010) Palustrine carbonates. In: Alonso-Zarza, A.M. & Tanner, L. (Eds.) *Carbonates in continental settings. Facies, environments and processes, Developments in Sedimentology*, 61. Oxford: Elsevier, pp. 103–131. [https://doi.org/10.1016/S0070-4571\(09\)06102-0](https://doi.org/10.1016/S0070-4571(09)06102-0)
- Alonso-Zarza, A.M., Meléndez, A., Martín-García, R., Herrero, M.J. & Martín-Pérez, A. (2012) Discriminating between tectonism and climate signatures in palustrine deposits: lessons from the Miocene of the Teruel Graben, NE Spain. *Earth Science Reviews*, 113, 141–160. <https://doi.org/10.1016/j.earscirev.2012.03.011>
- Alonso-Zarza, A.M., Cabaleri, N.G., Huerta, P., Armella, C., Rodríguez-Berriguete, Á., Monferran, M.D., Gallego, O.F.,

- Ubaldo, M.C. & Nieto, D.S. (2020) Lacustrine microbialite pinnacles in the Palaeogene of Patagonia, Argentina: facies and controls. *Sedimentary Geology*, 408, 105742. <https://doi.org/10.1016/j.sedgeo.2020.105742>
- Anadón, P. (1992) Lagos. In: Arche, A. (Ed.) *Sedimentología, Vol. I. Nuevas tendencias*. Madrid: Consejo Superior de Investigaciones Científicas, pp. 219–273.
- Andres, M.S., Sumner, D.Y., Reid, R.P. & Swart, P.K. (2006) Isotopic fingerprints of microbial respiration in aragonite from Bahamian stromatolites. *Geology*, 34(11), 973–976. <https://doi.org/10.1130/G22859A.1>
- Aragón, E. & Romero, E. (1984) Geología, paleoambientes y paleobotánica de yacimientos terciarios del occidente de Río Negro. Actas 9 Congreso Geológico Argentino, Buenos Aires, pp. 475–507.
- Aramendía, I., Bouza, P., Cuitiño, J., Raigemborn, M.S., González, F., Valenzuela, L., Babay, P. & Ghiglione, M. (2023) Paleoclimate from Miocene Paleosols in the northwestern edge of the Austral Magallanes Basin. Actas XVIII Reunión Argentina de Sedimentología y IX Congreso Latinoamericano de Sedimentología, La Plata, Buenos Aires, p. 268.
- Arche, A. (1992) Deltas. In: Arche, A. (Ed.) *Sedimentología, vol. I. Nuevas tendencias*. Madrid: Consejo Superior de Investigaciones Científicas, pp. 397–543.
- Arenas, C., Casanova, J. & Pardo, G. (1997) Stable-isotope characterization of the Miocene lacustrine systems of Los Monegros (Ebro Basin, Spain): palaeogeographic and palaeoclimatic implications. *Palaeogeography, Palaeoclimatology, Palaeoecology*, 128(1–4), 133–155. [https://doi.org/10.1016/S0031-0182\(96\)00052-1](https://doi.org/10.1016/S0031-0182(96)00052-1)
- Arenas, C. & Pardo, G. (1999) Latest Oligocene–Late Miocene lacustrine systems of the north-central part of the Ebro Basin (Spain): sedimentary facies model and palaeogeographic synthesis. *Palaeogeography, Palaeoclimatology, Palaeoecology*, 151(1–3), 127–148. [https://doi.org/10.1016/S0031-0182\(99\)00025-5](https://doi.org/10.1016/S0031-0182(99)00025-5)
- Arenas, C., Cabrera, L. & Ramos, L. (2007) Sedimentology and tufa facies and continental microbialites from the Palaeogene of Mallorca Island (Spain). *Sedimentary Geology*, 197(1–2), 1–22. <https://doi.org/10.1016/j.sedgeo.2006.08.009>
- Armenteros, I. (2010) Chapter 2: Diagenesis of carbonates in continental settings. In: Alonso-Zarza, A.M. & Tanner, L. (Eds.) *Carbonates in continental settings, geochemistry, diagenesis and applications, developments in sedimentology*, Vol. 62. Amsterdam, Netherlands: Elsevier, pp. 61–151. [https://doi.org/10.1016/S0070-4571\(09\)06202-5](https://doi.org/10.1016/S0070-4571(09)06202-5)
- Asensio, M., Cornu, M., Malumíán, N., Martínez, M. & Quattrocchio, M. (2010) Formación Río Foyel, Oligoceno de la Cuenca de Ñirihuau: la transgresión pacífica en la Cordillera Nordpatagónica. *Revista de la Asociación Geológica Argentina*, 66(3), 399–405.
- Asensio, M., Zavala, C. & Arcuri, M. (2004) Evidencias de la acción de mareas en la Cuenca de Ñirihuau. X Reunión Argentina de Sedimentología. Acta de resúmenes, pp. 19–21.
- Asensio, M., Zavala, C. & Arcuri, M. (2005) Los sedimentos terciarios del Río Foyel, provincia de Río Negro, Argentina. Actas 16 Congreso Geológico Argentino, La Plata, pp. 271–276.
- Asensio, M., Zavala, C. & Cazau, L. (2008) Análisis tectosedimentario de la Formación Salto del Macho, cuenca de Ñirihuau, Argentina. 7th Congreso de Exploración y Desarrollo de Hidrocarburos, Mar del Plata, Argentina, pp. 565–572.
- Astibia, H., López-Martínez, N., Elorza, J. & Vicens, E. (2012) Increasing size and abundance of microbialites (oncooids) in connection with the K/T boundary in non-marine environments in the South Central Pyrenees. *Geologica Acta*, 10(3), 209–226. <https://doi.org/10.1344/105.000001770>
- Awramik, S.M. & Riding, R. (1988) Role of algal eukaryotes in subtidal columnar stromatolite formation (cyanobacteria/Proterozoic/Shark Bay). *Proceedings of the National Academy of Sciences of the United States of America*, 85(5), 1327–1329. <https://doi.org/10.1073/pnas.85.5.1327>
- Barreda, V., Anzótegui, L.M., Prieto, A.R., Azeñolaza, P., Bianchi, M.M., Borromel, A.M., Brea, A.M., Caccavari, M., Cuadrado, G.A., Garralla, S., Grill, S., Guertstein, G.R., Lutz, A., Mancini, M.V., Mautino, L.R., Ottone, E.G., Quattrocchio, M.E., Romero, E.J., Zamaloa, M.C. & Zucol, A. (2007) Diversificación y cambios de las angiospermas durante el Neógeno en Argentina. *Ameghiniana*, Publicación Especial, 11, 173–191.
- Barreda, V., García, V.E., Quattrocchio, M.E. & Volkheimer, W. (2003) Palynostratigraphic analysis of the río Foyel formation (latest Oligocene–early Miocene), northwestern Patagonia, Argentina. *Revista Española de Micropaleontología*, 35(2), 229–239.
- Barreda, V. & Palazzesi, L. (2007) Patagonian vegetation turnovers during the Paleogene–Early Neogene: origin of arid adapted floras. *The Botanical Review*, 73, 31–50. [https://doi.org/10.1663/0006-8101\(2007\)73\[31:PVTDT\]2.0.CO;2](https://doi.org/10.1663/0006-8101(2007)73[31:PVTDT]2.0.CO;2)
- Barreda, V.D. & Palazzesi, L. (2021) Role of climate and tectonism on the modernization of Patagonian floras: Evidence from the fossil record. *Global and Planetary Change*, 204, 103556. <https://doi.org/10.1016/j.gloplacha.2021.103556>
- Bathurst, R.G.C. (1975) *Carbonate sediments and their diagenesis. Developments in sedimentology*. New York: Elsevier, p. 620.
- Bechis, F. (2004) Geología y estructura del sector medio de los ríos Ñirihuau y Pichi Leufú, provincia de Río Negro. Trabajo Final de Licenciatura, Universidad de Buenos Aires. Unpublished Thesis, p. 121.
- Bechis, F. & Cristallini, E. (2005) Tectonic evolution of Northern Ñirihuau Basin, Northwestern Patagonia, Argentina. 6 International Symposium of Andean Geodynamics (ISAG), Barcelona, España, pp. 103–106.
- Bechis, F. & Cristallini, E. (2006) Inflexiones en estructuras del sector norte de la faja plegada y corrida de Ñirihuau, provincia de Río Negro. *Revista de la Asociación Geológica Argentina*, 25, 18–25.
- Bechis, F., Encinas, A., Litvak, V.D., Valencia, V. & Ramos, V.A. (2014a) Nuevas edades U-Pb del relleno de la cuenca de Ñirihuau, Andes Nordpatagónicos. Actas 19° n. Congreso Geológico Argentino, Córdoba, pp. 15698–15699.
- Bechis, F., Encinas, A., Concheyro, A., Litvak, V.D., Aguirre-Urreta, B. & Ramos, V.A. (2014b) New age constraints for the Cenozoic marine transgressions of north- western Patagonia, Argentina (41°–43°S): paleogeographic and tectonic implications. *Journal of South American Earth Sciences*, 52, 72–93. <https://doi.org/10.1016/j.jsames.2014.02.003>
- Bechis, F., Encinas, A., Valencia, V.A. & Ramos, V.A. (2015) Analyzing the transition from extension to contraction at the North Patagonian Andes. Actas 14° Congreso Geológico Chileno, La Serena, pp. 737–739.
- Benavente, C.A., Mancuso, A.C. & Cabaleri, N.G. (2012) First occurrence of charophyte algae from a Triassic paleolake in Argentina

- and their paleoenvironmental context. *Paleogeography, Palaeoclimatology, Palaeoecology*, 363–364, 172–183. <https://doi.org/10.1016/j.palaeo.2012.09.016>
- Benavente, C.A., Mancuso, A.C. & Bohacs, K.M. (2019) Paleohydrogeologic reconstruction of Triassic carbonate paleolakes from stable isotopes: encompassing two lacustrine models. *Journal of South American Earth Sciences*, 95, 102292. <https://doi.org/10.1016/j.jsames.2019.102292>
- Benavente, C.A., Mancuso, A.C., Irmis, R.B., Bohacs, K.M. & Matheos, S. (2021) Tectonically conditioned record of continental interior paleoclimate during the Carnian pluvial event: the Upper Triassic Los Rastros Formation, Argentina. *Geological Society of America Bulletin*, 134(1–2), 60–80. <https://doi.org/10.1130/B35847.1>
- Benavente, C.A., Matheos, S., Barredo, S., Abarzúa, F. & Mancuso, A.C. (2023) Diagenesis of continental carbonates linked to the evolution of the flexural margin of the Sorocayense-Hilario subbasin, Argentina. *Andean Geology*, 50(2), 269–290. <https://doi.org/10.5027/andgeoV50n2-3450>
- Bertels, A. & Cusminsky, G.C. (1995) Ostrácodos de la Formación Ñirihuau (Oligoceno), Cuenca de Ñirihuau-Ñorquinco-Cushamen: Significado paleoambiental. *Publicación Electrónica de la Asociación Paleontológica Argentina*, 3(1), 23–25.
- Bertels-Psotka, A. & Cusminsky, G.C. (1999) Nuevas especies de ostrácodos de la Formación Ñirihuau (Oligoceno) en su área tipo (alrededores de San Carlos de Bariloche), provincia de Río Negro, República Argentina. *Ameghiniana*, 36(1), 71–81.
- Bhattacharya, J.P. (2006) Deltas. In: Posamentier, H.W. & Walker, R.G. (Eds.) *Facies models revisited*, Vol. 84. Tulsa, Oklahoma, USA: SEPM Special Publication, pp. 237–292.
- Bilmes, A., Veiga, G.D. & Franzese, J.R. (2014) Relleno intermontano en el Antepaís Fragmentado Patagónico: evolución neógena de la Cuenca de Gastre. *Revista de la Asociación Geológica Argentina*, 71(3), 311–330.
- Bocchino, R.A. (1964) Sobre un Pygidiidae (Pisces, Siluriformes) del Eoceno de Río Negro. *Ameghiniana*, 3(7), 185–189.
- Bohacs, K.M., Carroll, A.R., Neal, J.E. & Mankiewicz, P.J. (2000) Lake-basin type, source potential, and hydrocarbon character: an integrated sequence-stratigraphic-geochemical framework. In: Gierlowski-Kordesch, E. & Kelts, K. (Eds.) *Lake basins through space and time*, Vol. 46. United Kingdom: American Association of Petroleum Geologists Studies in Geology, pp. 3–37.
- Bohacs, K.M., Carroll, A.R. & Neal, J.E. (2003) Lessons from large lake systems—Thresholds, nonlinearity, and strange attractors. In: Chan, M.A. & Archer, A.W. (Eds.) *Extreme depositional environments: mega end members in geologic time*, Vol. 370. USA: Geological Society of America Special Paper, pp. 75–90. <https://doi.org/10.1130/0-8137-2370-1.75>
- Bohacs, K.M. & Suter, J. (1997) Sequence stratigraphic distribution of coaly rocks: Fundamental controls and paralic examples. *Bulletin of American Association of Petroleum Geologists*, 10(81), 1612–1639. <https://doi.org/10.1306/3B05C3FC-172A-11D7-8645000102C1865D>
- Bourillot, R., Vennin, E., Dupraz, C., Pace, A., Foubert, A., Rouchy, J.M., Patrier, P., Blanc, P., Bernard, D. & Lesseur, J. (2020) The record of environmental and microbial signatures in ancient microbialites: the terminal carbonate complex from the Neogene Basins of Southeastern Spain. *Minerals*, 10(3), 276. <https://doi.org/10.3390/min10030276>
- Braga, J.C., Martín, J.M. & Riding, R. (1995) Controls on microbial dome fabric development along a carbonate-siliciclastic shelf-basin transect, Miocene, SE Spain. *Palaios*, 10(4), 347–361. <https://doi.org/10.2307/3515160>
- Bucher, J., Varela, A., D'Elia, L., Bilmes, A., López, M., García, M. & Franzese, J. (2020) Multiproxy paleosol evidence for a rain shadow effect linked to Miocene uplift of the North Patagonian Andes. *GSA Bulletin*, 132(7–8), 1603–1614. <https://doi.org/10.1130/B35331.1>
- Bucher, J., Pérez, M.E., Ruiz, L.R.G., D'Elia, L. & Bilmes, A. (2021) New middle Miocene (Langhian–Serravallian) vertebrate localities in northwestern Patagonia, Argentina: a contribution to high latitude south american land mammal ages sequence. *Journal of South American Earth Sciences*, 107, 103024. <https://doi.org/10.1016/j.jsames.2020.103024>
- Burne, R.V. & Moore, L.S. (1987) Microbialites: organo-sedimentary deposits of benthic microbial communities. *Palaios*, 2(3), 241–245. <https://doi.org/10.2307/3514674>
- Butler, K.L., Horton, B.K., Echaurren, A., Folguera, A. & Fuentes, F. (2020) Cretaceous–Cenozoic growth of the Patagonian broken foreland basin, Argentina: chronostratigraphic framework and provenance variations during transitions in Andean subduction dynamics. *Journal of South American Earth Sciences*, 97, 102242. <https://doi.org/10.1016/j.jsames.2019.102242>
- Camoin, G., Casanova, J., Rouchy, J.M., Blanc-Valleron, M.M. & Deconinck, J.F. (1997) Environmental controls on perennial and ephemeral carbonate lakes: the central palaeo-Andean Basin of Bolivia during Late Cretaceous to early Tertiary times. *Sedimentary Geology*, 113(1–29), 1–26. [https://doi.org/10.1016/S0037-0738\(97\)00052-3](https://doi.org/10.1016/S0037-0738(97)00052-3)
- Carrapa, B., Clementz, M. & Feng, R. (2019) Ecological and hydroclimate responses to strengthening of the Hadley circulation in South America during the Late Miocene cooling. *Proceedings of the National Academy of Sciences of the United States of America*, 116(20), 9747–9752. <https://doi.org/10.1073/pnas.1810721116>
- Carroll, A.R. & Bohacs, K.M. (1999) Stratigraphic classification of ancient lakes: balancing tectonic and climatic controls. *Geology*, 27(2), 99–102. [https://doi.org/10.1130/0091-7613\(1999\)027<0099:SCOALB>2.3.CO;2](https://doi.org/10.1130/0091-7613(1999)027<0099:SCOALB>2.3.CO;2)
- Caviglia, N. & Zamaloa, M.D.C. (2014) Flora angiospérmica de Pico Quemado, formación Ñirihuau (Oligoceno Tardío), provincia de Río Negro, Argentina. *Ameghiniana*, 51(3), 209–225.
- Caviglia, N. (2018) Early Miocene climate estimations in Patagonia: the case of Pico Quemado, Ñirihuau Formation (Lower–Middle Miocene). *Journal of South American Earth Sciences*, 88, 64–71. <https://doi.org/10.1016/j.jsames.2018.08.002>
- Cazau, L.B. (1972) Cuenca de Ñirihuau-Ñorquinco-Cushamen. In: Leanza, A. (Ed.) *Geología Regional Argentina*. Córdoba, Argentina: Academia Nacional de Ciencias de Córdoba, pp. 727–740.
- Cazau, L.B. (1980) Cuenca de Ñirihuau-Ñorquinco-Cushamen. In: Turner, J.C. (Ed.) *Geología regional Argentina*. Córdoba, Argentina: Academia Nacional de Ciencias de Córdoba, pp. 1149–1171.
- Cazau, L.B., Mancini, D., Cangini, J. & Spalletti, L.A. (1989) Cuenca de Ñirihuau. In: Chebli, G.A. & Spalletti, L.A. (Eds.) *Cuencas Sedimentarias Argentinas*, Vol. 6. Tucumán, Argentina: Serie Correlación Geológica, pp. 299–318.
- Cazau, L.B., Cortiñas, J., Reinante, S., Asensio, M., Bechis, F. & Aprea, D. (2005) Cuenca de Ñirihuau. In: Chebli, G.A.,

- Cortiñas, J., Spalletti, L.A., Legarreta, L. & Vallejo, E.L. (Eds.) *Frontera Exploratoria de la Argentina*, 6 Congreso de Exploración y Desarrollo de Hidrocarburos. Argentina: Mar del Plata, pp. 251–273.
- Chafetz, H.S. & Buczynski, C. (1992) Bacterially induced lithification of microbial mats. *Palaios*, 7, 277–293. <https://doi.org/10.2307/3514973>
- Christ, N., Maerz, S., Kutschera, E., Kwiecień, O. & Mutti, M. (2018) Palaeoenvironmental and diagenetic reconstruction of a closed-lacustrine carbonate system—the challenging marginal setting of the Miocene Ries Crater Lake (Germany). *Sedimentology*, 65, 235–262. <https://doi.org/10.1111/sed.12401>
- Cione, A.L. & Báez, A.M. (2007) Peces continentales y anfibios cenozoicos de Argentina los últimos cincuenta años. *Ameghiniana*, Publicación Especial, 11(1), 195–220.
- Cohen, A.S. (2003) *Paleolimnology: The history and evolution of lake systems*. Oxford: Oxford University Press, p. 528.
- Collinson, J.D. & Thompson, D.B. (1989) *Sedimentary structures*. London: Chapman & Hall, p. 207.
- Compagnucci, R.H. (2011) Atmospheric circulation over Patagonia from the Jurassic to present: a review through proxy data and climatic modelling scenarios. *Biological Journal of the Linnean Society*, 103(2), 229–249. <https://doi.org/10.1111/j.1095-8312.2011.01655.x>
- Choquette, P.W. & James, N.P. (1987) Diagenesis 12. Limestone-3. The deep burial environment. *Geoscience Canada*, 14(1), 3–35.
- Davis, S.J., Mulch, A., Carroll, A.R., Horton, T.W. & Chamberlain, C.P. (2009) Paleogene landscape evolution of the central North American Cordillera: developing topography and hydrology in the Laramide foreland. *Geological Society of America Bulletin*, 121(1–2), 100–116. <https://doi.org/10.1130/B26308.1>
- De Deckker, P. & Forester, R.M. (1988) The use of ostracods to reconstruct continental palaeoenvironmental records. In: De Deckker, P., Colin, J.P. & Peyrouquet, J.P. (Eds.) *Ostracoda in the earth sciences*. Amsterdam: Elsevier, pp. 175–199.
- Deocampo, D.M. (2010) The geochemistry of continental carbonates. In: Alonso-Zarza, A.M. & Tanner, L.H. (Eds.) *Carbonates in continental settings: geochemistry, diagenesis and applications*, Vol. 62. Amsterdam: Elsevier, pp. 1–59. [https://doi.org/10.1016/S0070-4571\(09\)06201-3](https://doi.org/10.1016/S0070-4571(09)06201-3)
- Diez, O.M. & Zubia, M.A. (1981) Sinopsis estratigráfica de la región de “El Bolsón”, provincia de Río Negro. *Revista de la Asociación Geológica Argentina*, 36(1), 19–28.
- Druschke, P.A., Jiang, G., Anderson, T.B. & Hanson, A.D. (2009) Stromatolites in the Late Ordovician Eureka Quartzite: implications for microbial growth and preservation in siliciclastic settings. *Sedimentology*, 56, 1275–1291. <https://doi.org/10.1111/j.1365-3091.2008.01033.x>
- Dunn, R.E., Strömberg, C.A., Madden, R.H., Kohn, M.J. & Carlini, A.A. (2015) Linked canopy, climate, and faunal change in the Cenozoic of Patagonia. *Science*, 347(6219), 258–261. <https://doi.org/10.1126/science.1260947>
- Dunham, R.J. (1962) Classification of carbonate rocks according to depositional texture. In: Ham, W.E. (Ed.) *Classification of carbonate rocks*. Tulsa, Oklahoma, USA: American Association of Petroleum Geologists, pp. 108–121.
- Dupraz, C., Visscher, P.T., Baumgartner, L.K. & Reid, R.P. (2004) Microbe–mineral interactions: early carbonate precipitation in a hypersaline lake (Eleuthera Island, Bahamas). *Sedimentology*, 51(4), 745–765. <https://doi.org/10.1111/j.1365-3091.2004.00649.x>
- Dupraz, C., Reid, R.P., Braissant, O., Decho, A.W., Norman, R.S. & Visscher, P.T. (2009) Processes of carbonate precipitation in modern microbial mats. *Earth Science Reviews*, 96(3), 141–162. <https://doi.org/10.1016/j.earscirev.2008.10.005>
- Emiliani, C. & Edwards, G. (1953) Tertiary ocean bottom temperatures. *Nature*, 171(4359), 887–888. <https://doi.org/10.1038/171887c0>
- Fabrezi, M. (2006) Morphological evolution of Ceratophryinae (Anura, Neobatrachia). *Journal of Zoology, Systematics and Evolutionary Research*, 44(2), 153–166. <https://doi.org/10.1111/j.1439-0469.2005.00349.x>
- Falaschi, P., Zamalao, M.D.C., Caviglia, N. & Romero, E.J. (2012) Flora gimnospérmica de la Formación Ñirihua (Oligoceno Tardío-Mioceno Temprano), provincia de Río Negro, Argentina. *Ameghiniana*, 49(4), 525–551.
- Fernández Paz, L., Bechis, F., Litvak, V.D., Echaurren, A., Encinas, A., González, J., Lucassen, F., Oliveros, V., Valencia, V. & Folguera, A. (2019) Constraints on trenchward arc migration and backarc magmatism in the North Patagonian Andes in the context of Nazca Plate Rollback. *Tectonics*, 38(11), 3794–3817. <https://doi.org/10.1029/2019TC005580>
- Feruglio, E. (1941) Nota preliminar sobre la hoja geológica “San Carlos de Bariloche” (Patagonia), 200. *Boletín de Informaciones Petroleras*, 18(200), 27–64.
- Flower, B.P. & Kennett, J.P. (1994) The middle Miocene climatic transition: East Antarctic ice sheet development, deep ocean circulation and global carbon cycling. *Palaeogeography, Palaeoclimatology, Palaeoecology*, 108(3–4), 537–555. [https://doi.org/10.1016/0031-0182\(94\)90251-8](https://doi.org/10.1016/0031-0182(94)90251-8)
- Flügel, E. (2010) *Microfacies of carbonate rocks: analysis, interpretation and application*, 2nd edition. Berlin, Heidelberg: Springer, p. 984. <https://doi.org/10.1007/978-3-642-03796-2>
- Freytet, P. & Verrecchia, E.P. (1998) Freshwater organisms that build stromatolites: a synopsis of biocrystallization by prokaryotic and eukaryotic algae. *Sedimentology*, 45(3), 535–563. <https://doi.org/10.1046/j.1365-3091.1998.00155.x>
- Frost, D.R., Grant, T., Faivovich, J., Bain, R.H., Haas, A., Haddad, C.F.B., De Sá, R.O., Channing, A., Wilkinson, M., Donnellan, S.C., Raxworthy, C.J., Campbell, J.A., Blotto, B.L., Moler, P., Drewes, R.C., Nussbaum, R.A., Lynch, J.D., Green, D.M. & Wheeler, W.C. (2006) The amphibian tree of life. *Bulletin of the American Museum of Natural History*, 297, 1–291. [https://doi.org/10.1206/0003-0090\(2006\)297\[0001:TATOL\]2.0.CO;2](https://doi.org/10.1206/0003-0090(2006)297[0001:TATOL]2.0.CO;2)
- García Morabito, E., Beltrán-Triviño, A., Terrizzano, C.M., Bechis, F., Likerman, J., Von Quadt, A. & Ramos, V.A. (2021) The influence of climate on the dynamics of mountain building within the northern Patagonian Andes. *Tectonics*, 40(2). Portico. <https://doi.org/10.1029/2020tc006374>
- Giacosa, R. & Heredia, N. (1999) La cuenca de antepaís terciaria asociada a la faja plegada y corrida de los Andes Patagónicos entre los 41° y 42° SSO de Argentina. *Acta Geológica Hispánica*, 32(1–2), 103–111.
- Giacosa, R. & Heredia, N. (2004) Structure of the North Patagonian thick-skinned fold-and-thrust belt, southern central Andes, Argentina (41°–42°S). *Journal of South American Earth Sciences*, 18(1), 61–72. <https://doi.org/10.1016/j.jsames.2004.08.006>
- Giacosa, R., Heredia, N., Césari, O., Zubia, M., González, R. & Faroux, A. (2001) Descripción geológica de la Hoja 4172-IV, San Carlos de Bariloche, provincias de Río Negro y Neuquén.

- Servicio Geológico Minero Argentino, Instituto de Geología y Recursos Minerales, Boletín 279, Buenos Aires.
- Giacosa, R.E., Alfonso, J.C., Heredia, N. & Paredes, J. (2005) Tertiary tectonics of the sub-Andean region of the North Patagonian Andes, southern central Andes of Argentina (41–42°30' S). *Journal of South American Earth Sciences*, 20(3), 157–170. <https://doi.org/10.1016/j.jsames.2005.05.013>
- Gierlowski-Kordesch, E.H. (1998) Carbonate deposition in an ephemeral siliciclastic alluvial system: Jurassic Shuttle Meadow Formation, Newark Supergroup, Hartford Basin, USA. *Paleogeography, Palaeoclimatology, Palaeoecology*, 140(1–4), 161–184. [https://doi.org/10.1016/S0031-0182\(98\)00039-X](https://doi.org/10.1016/S0031-0182(98)00039-X)
- Gierlowski-Kordesch, E. & Kelts, K. (1994) *Global geological record of lake basins*, Vol. 1. New York, USA: Cambridge University Press, p. 427.
- Gierlowski-Kordesch, E.H., Gomez Fernandez, J.C. & Melendez, N. (1991) Carbonate and coal deposition in an alluvial-lacustrine setting: Lower Cretaceous (Weald) in the Iberian Range (east-central Spain). In: Anadón, P., Cabrera, L. & Kelts, K. (Eds.) *Lacustrine facies analysis*, Vol. 13. Blackwell, Oxford: Special Publication International Association of Sedimentologists, pp. 109–125. <https://doi.org/10.1002/9781444303919.ch6>
- Gierlowski-Kordesch, E.H. (2010) Chapter 1: lacustrine carbonates. In: Alonso-Zarza, A.M. & Tanner, L.H. (Eds.) *Carbonates in continental settings: facies, environments and processes, Developments in sedimentology*, Vol. 61. Amsterdam, Netherlands: Elsevier, pp. 1–101. [https://doi.org/10.1016/S0070-4571\(09\)06101-9](https://doi.org/10.1016/S0070-4571(09)06101-9)
- Goddard, E.N., Trask, P.D., De Ford, R.K., Rove, O.N., Singewald, J.T., Jr. & Overbeck, R.M. (1948) *Rock-color chart*. USA: Geological Society of America, reprinted 1984.
- González, P., Coluccia, A. & Franchi, M. (2000) Hoja Geológica 4169-III Ingeniero Jacobacci. Provincia de Río Negro. In: *Programa Nacional de Cartas Geológicas de la República Argentina 1:250.000*, Vol. 311. Boletín, Buenos Aires: Servicio Geológico Minero Argentino.
- González Bonorino, F. (1973) Geología del área entre San Carlos de Bariloche y Llao-Llao. *Fundación Bariloche, Departamento de Recursos Naturales y Energía, Publicación*, 16, 1–53.
- González Bonorino, F. (1944) Descripción geológica y petrográfica de la Hoja geológica 41b río Foyel (Río Negro). *Dirección Nacional Minería e Hidrogeología, Boletín*, 56, 124.
- González Bonorino, F. & González Bonorino, G. (1978) Geología de la región de San Carlos de Bariloche: un estudio de las formaciones terciarias del Grupo Nahuel Huapi. *Revista de la Asociación Geológica Argentina*, 33(3), 175–210.
- Grotzinger, J.P. & Knoll, A.H. (1995) Anomalous carbonate precipitates: is the Precambrian the key to the Permian? *Palaos*, 10(6), 578–596. <https://doi.org/10.2307/3515096>
- Guo, L., Andrews, J., Riding, R., Dennis, P. & Dresser, Q. (1996) Possible microbial effects on stable carbon isotopes in hot-spring travertines. *Journal of Sedimentary Research*, 66(3), 468–473. <https://doi.org/10.1306/D4268379-2B26-11D7-8648000102C1865D>
- Håkanson, L. (2007) Lake environments. In: Perry, C. & Taylor, K. (Eds.) *Environmental sedimentology*. Oxford, UK: Blackwell Publishing, pp. 109–143.
- Harms, J.C., Southard, J.B. & Walker, R.G. (1982) *Structures and sequences in clastic rocks*. USA: SEPM Society for Sedimentary Geology, SEPM Short Course Notes, vol. 9, p. 51.C. <https://doi.org/10.2110/scn.82.09>
- Henkes, G.A., Passey, B.H., Grossman, E.L., Shenton, B.J., Yancey, T.E. & Pérez-Huerta, A. (2018) Temperature evolution and the oxygen isotope composition of Phanerozoic oceans from carbonate clumped isotope thermometry. *Earth and Planetary Science Letters*, 490, 40–50. <https://doi.org/10.1016/j.epsl.2018.02.001>
- Hiatt, E.E. & Pufahl, P.K. (2014) Cathodoluminescence petrography of carbonate rocks: application to understanding diagenesis, reservoir quality, and pore system evolution. In: Coulson, I. (Ed.) *Cathodoluminescence and its application to geoscience*. Short Course Series, Vol. 45. Fredericton, NB, Canadá: Mineralogical Association of Canada, pp. 75–96.
- Hinojosa, L.F. (2005) Cambios climáticos y vegetacionales inferidos a partir de paleofloras cenozoicas del sur de Sudamérica. *Revista Geológica de Chile*, 32(1), 95–115. <https://doi.org/10.4067/S0716-02082005000100006>
- Hinojosa, L.F. & Villagrán, C. (2005) Did South American mixed paleofloras evolve under thermal equability or in the absence of an effective Andean barrier during the Cenozoic? *Paleogeography, Paleoclimatology, Paleoeology*, 217(1–2), 1–23. <https://doi.org/10.1016/j.palaeo.2004.11.013>
- Hinojosa, L.F. & Gutiérrez, N. (2009) Cambio climático y diversidad: El caso de la Formación Navidad, Mioceno de Chile central. XXII Congreso Geológico Chileno, Santiago, Chile, p. 4.
- Horita, J. & Wesolowski, D.J. (1994) Liquid-vapor fractionation of oxygen and hydrogen isotopes of water from the freezing to the critical temperature. *Geochimica et Cosmochimica*, 58(16), 3425–3437. [https://doi.org/10.1016/0016-7037\(94\)90096-5](https://doi.org/10.1016/0016-7037(94)90096-5)
- Icole, M., Masse, J.P., Perinet, G. & Taieb, M. (1990) Pleistocene lacustrine stromatolites, composed of calcium carbonate, fluoride, and dolomite, from Lake Natron, Tanzania: depositional and diagenetic processes and their paleoenvironmental significance. *Sedimentary Geology*, 69(1–2), 139–155. [https://doi.org/10.1016/0037-0738\(90\)90105-3](https://doi.org/10.1016/0037-0738(90)90105-3)
- Iglesias, A.R.I., Artabe, A.E. & Morel, E.M. (2011) The evolution of Patagonian climate and vegetation from the Mesozoic to the present. *Biological Journal of the Linnean Society*, 103(2), 409–422. <https://doi.org/10.1111/j.1095-8312.2011.01657.x>
- Jordan, T.E., Matthew Burns, W., Veiga, R., Pangaro, F., Copeland, P., Kelley, S. & Mpodozis, C. (2001) Extension and basin formation in the Southern Andes caused by increased convergence rate: a mid-Cenozoic trigger for the Andes. *Tectonics*, 20(3), 308–324. <https://doi.org/10.1029/1999TC001181>
- Kelts, K. & Talbot, M. (1990) Lacustrine carbonates as geochemical archives of environmental change and biotic/abiotic interactions. In: Tilzer, M.M. & Serruya, C. (Eds.) *Large Lakes: ecological structure and function*. Brock/Springer Series in Contemporary Bioscience. Berlin, Heidelberg: Springer, pp. 288–315. https://doi.org/10.1007/978-3-642-84077-7_15
- Kennard, J.M. & Burne, R.V. (1989) *Stromatolite newsletter number 14*. Canberra: Bureau of Mineral Resources, Geology and Geophysics, p. 179.
- Kent-Corson, M.L., Mulch, A., Graham, S.A., Carroll, A.C., Ritts, B.D. & Chamberlain, C.P. (2010) Diachronous isotopic and sedimentary responses to topographic change as indicators of mid-Eocene hydrologic reorganization in the western United States. *Basin Research*, 22(6), 829–845. <https://doi.org/10.1111/j.1365-2117.2009.00456.x>
- Knorr, G., Butzin, M., Micheels, A. & Lohmann, G. (2011) A warm Miocene climate at low atmospheric CO₂ levels. *Geophysical*

- Research Letters*, 38(20), L20701. <https://doi.org/10.1029/2011GL048873>
- Kohn, M.J., Wieland, M.S., Parkinson, C.D. & Upreti, B.N. (2015) Quasi-static Eocene–Oligocene climate in Patagonia promotes slow faunal evolution and mid-Cenozoic global cooling. *Palaeogeography, Palaeoclimatology, Palaeoecology*, 435, 24–37. <https://doi.org/10.1016/j.palaeo.2015.05.028>
- Lamb, A.L., Leng, M.J., Lamb, H.F. & Mohammed, M.U. (2000) A 9000-year oxygen and carbon isotope record of hydrological change in small Ethiopian Crater Lake. *The Holocene*, 10(2), 167–177. <https://doi.org/10.1191/095968300677444>
- Le Roux, J.P. (2012) A review of tertiary climate changes in southern South America and the Antarctic Peninsula. Part 2: continental conditions. *Sedimentary Geology*, 247–248, 21–38. <https://doi.org/10.1016/j.sedgeo.2011.12.001>
- Leng, M.J. & Marshall, J.D. (2004) Paleoclimatic interpretation of stable isotope data from lake sediment archives. *Quaternary Science Reviews*, 23(7–8), 811–831. <https://doi.org/10.1016/j.quascirev.2003.06.012>
- Leng, M.J., Lamb, A.L., Heaton, T.H.E., Marshall, J.D., Wolfe, B.B., Jones, M.D., Holmes, J.A. & Arrowsmith, A. (2005) Isotopes in lake sediments. In: Leng, M.J. (Ed.) *Isotopes in palaeoenvironmental research*. The Netherlands: Springer, pp. 147–184. https://doi.org/10.1007/1-4020-2504-1_04
- Leutert, T.J., Modestou, S., Bernasconi, S.M. & Meckler, A.N. (2021) Southern Ocean bottom-water cooling and ice sheet expansion during the middle Miocene climate transition. *Climate of the Past*, 17(5), 2255–2271. <https://doi.org/10.5194/cp-17-2255-2021>
- Link, M.H., Osborne, R.H. & Awramik, S.M. (1978) Lacustrine stromatolites and associated sediments of the Pliocene ridge route formation, ridge basin, California. *Journal of Sedimentary Research*, 48(1), 143–157. <https://doi.org/10.1306/212F7414-2B24-11D7-8648000102C1865D>
- Logan, B.W., Rezak, R. & Ginsburg, R.N. (1964) Classification and environmental significance of algal stromatolites. *The Journal of Geology*, 72(1), 68–83. <https://doi.org/10.1086/626965>
- Lüdecke, T., Mikes, T., Rojay, F.B., Cosca, M.A. & Mulch, A. (2013) Stable isotope-based reconstruction of Oligo-Miocene paleoenvironment and paleohydrology of Central Anatolian lake basins (Turkey). *Turkish Journal of Earth Sciences*, 22(5), 793–819. <https://doi.org/10.3906/yer-1207-11>
- MacFadden, B.J., Cerling, T.E. & Prado, J. (1996) Cenozoic terrestrial ecosystem evolution in Argentina: evidence from carbon isotopes of fossil mammal teeth. *Palaios*, 11(4), 319–327. <https://doi.org/10.2307/3515242>
- Machado, M.A., Passalia, M.G., Vera, E.I., Santonja, C., Suriano, J. & Bechis, F. (2022) Registro megafloístico en la localidad Cordón de Las Bayas, sección inferior de la Formación Ñirihuau (Mioceno inferior-medio), provincia de Río Negro, Argentina. Reunión de comunicaciones de la Asociación Paleontológica Argentina. Salta Argentina, Libro de Resúmenes, p. 164.
- Machado, M.A., Yañez, A., Passalia, M.G., Santonja, C., Vera, E.I., Suriano, J. & Bechis, F. (2024) Pteridium (Dennstaedtiaceae) from Miocene of Patagonia (Río Negro, Argentina): the southernmost evidence of bracken fern in South America. *Historical Biology*, 1–16. <https://doi.org/10.1080/08912963.2024.2324442>
- Machel, H.G. (2000) Application of cathodoluminescence to carbonate diagenesis (chapter 11). In: Pagel, M., Barbin, V., Blanc, P. & Ohnenstetter, D. (Eds.) *Cathodoluminescence in geosciences*. Berlin, Heidelberg: Springer, pp. 271–301. https://doi.org/10.1007/978-3-662-04086-7_11
- Malumián, N. & Náñez, C. (2011) The Late Cretaceous–Cenozoic transgressions in Patagonia and the Fuegian Andes: foraminifera, palaeoecology, and palaeogeography. *Biological Journal of the Linnean Society*, 103(2), 269–288. <https://doi.org/10.1111/j.1095-8312.2011.01649.x>
- Mancini, D. & Serna, M. (1989) Evaluación petrolera de la Cuenca de Ñirihuau. Sudoeste de Argentina. Actas 1 Congreso Nacional de Exploración de Hidrocarburos, Buenos Aires, Argentina, pp. 739–762.
- Mariano, A.N. (1988) Some further geological applications of cathodoluminescence. In: Marshall, J.D. (Ed.) *Cathodoluminescence of geological materials*. Boston, MA: Unwin Hyman, pp. 94–123.
- Marshall, J.D. (1988) *Cathodoluminescence of geological materials*. Boston, MA: Unwin Hyman, p. 146.
- Matthews, R.K. & Poore, R.Z. (1981) Oxygen isotope record of ice volume history: 100 my of Glacio-Eustatic sea level fluctuation. *Bulletin of American Association of Petroleum Geologists*, 65(5), 954.
- Miall, A.D. (1978) Lithofacies types and vertical profile models of braided river deposits, a summary. In: Miall, A.D. (Ed.) *Fluvial sedimentology*, Vol. 5. Calgary: Memoir Canadian Society Petrology Geology, pp. 597–604.
- Miall, A.D. (1996) *The geology of fluvial deposits. Sedimentary facies, basin analysis, and petroleum geology*. New York: Springer-Verlag, p. 582.
- Miller, K.G. & Katz, M.E. (1987) Oligocene to Miocene benthic foraminiferal and abyssal circulation changes in the North Atlantic. *Micropaleontology*, 33(2), 97–149. <https://doi.org/10.2307/1485489>
- Murphy, J.T., Jr., Lowenstein, T.K. & Pietras, J.T. (2014) Preservation of primary lake signatures in alkaline earth carbonates of the Eocene Green River Wilkins Peak-Laney Member transition zone. *Sedimentary Geology*, 314, 75–91. <https://doi.org/10.1016/j.sedgeo.2014.09.005>
- Nichols, G. (2009) *Sedimentology and stratigraphy*. United Kingdom: John Wiley & Sons, p. 432.
- Ortiz-Jaureguizar, E. & Cladera, G.A. (2006) Paleoenvironmental evolution of southern South America during the Cenozoic. *Journal of Arid Environments*, 66(3), 498–532. <https://doi.org/10.1016/j.jaridenv.2006.01.007>
- Orts, D., Folguera, A., Giménez, M., Ruiz, F., Rojas Vera, E. & Lince Klinger, F. (2015) Cenozoic building and deformational processes in the North Patagonian Andes. *Journal of Geodynamics*, 86, 26–41. <https://doi.org/10.1016/j.jog.2015.02.002>
- Palazzesi, L. & Barreda, V. (2012) Fossil pollen records reveal a late rise of open-habitat ecosystems in Patagonia. *Nature Communications*, 3(1), 1294. <https://doi.org/10.1038/ncomm52299>
- Pardo-Casas, F. & Molnar, P. (1987) Relative motion of the Nazca (Farallon) and South American plates since Late Cretaceous time. *Tectonics*, 6(3), 233–248. <https://doi.org/10.1029/TC006i003p00233>
- Paredes, J.M., Giacosa, R.E. & Heredia, N. (2009) Sedimentary evolution of Neogene continental deposits (Ñirihuau Formation) along the Ñirihuau river, North Patagonian Andes of Argentina. *Journal of South American Earth Sciences*, 28(1), 74–88. <https://doi.org/10.1016/j.jsames.2009.01.002>
- Parrish, J.T., Hyland, E.G., Chan, M.A. & Hasiotis, S.T. (2019) Stable and clumped isotopes in desert carbonate spring and lake

- deposits reveal palaeohydrology: a case study of the Lower Jurassic Navajo Sandstone, south-western USA. *Sedimentology*, 66(1), 32–52. <https://doi.org/10.1111/sed.12540>
- Pascual, R., Bondesio, P., Vucetich, M.G., Scillato Yané, G.J., Bond, M. & Tonni, E.P. (1984) Vertebrados fósiles cenozoicos. Capítulo II-9. IX Congreso Geológico Argentino (San Carlos de Bariloche), Relatorio, pp. 439–461.
- Passalía, M.G. & Bechis, F. (2012) Megafloras de la sección basal de la Formación Ñirihuau (Oligoceno Superior?–Mioceno Inferior) en las localidades Pico Quemado y Cordón de las Bayas, provincia de Río Negro, Argentina. 15 *Símpoio Argentino de Paleobotánica y Palinología*. Corrientes, Resúmenes en CD-ROM.
- Passalía, M.G., Barreda, V., Bechis, F., Panti, C. & Caviglia, N. (2016) New micro- and megafloral records from the upper section of Ñirihuau Formation (middle Miocene), Río Negro Province, Argentina. 11 Congreso de la Asociación Paleontológica Argentina. Roca, Río Negro, Argentina, Libro de Resúmenes, pp. 76–77.
- Passalía, M.G., Caviglia, N. & Vera, E. (2019) *Lithraea australis* (Berry) comb. nov. (Anacardiaceae) from the upper section of Ñirihuau Formation (middle Miocene), Patagonia. *Review of Palaeobotany and Palynology*, 266, 1–11. <https://doi.org/10.1016/j.revpalbo.2019.04.003>
- Platt, N.H. (1989) Lacustrine carbonates and pedogenesis: sedimentology and origin of palustrine deposits from the Early Cretaceous Rupelo Formation, W Cameros Basin, N Spain. *Sedimentology*, 36(4), 665–684. <https://doi.org/10.1111/j.1365-3091.1989.tb02092.x>
- Platt, N. & Wright, P. (1991) Lacustrine carbonates: facies models, facies distributions and hydrocarbon aspects. In: Anadón, P., Cabrera, L. & Kelts, K. (Eds.) *Lacustrine facies analysis*, Vol. 13. Special Publication of the International Association of Sedimentologists. Oxford, UK: Blackwell Scientific Publishing, pp. 57–74. <https://doi.org/10.1002/9781444303919.ch3>
- Posamentier, H.W. & Walker, R.G. (2006) *Facies models revisited*, Vol. 84. Tulsa, Oklahoma, USA: SEPM Society for Sedimentary Geology Special Publication. <https://doi.org/10.2110/pec.06.84>
- Potter, J., Siemann, M.G. & Tsygukov, M. (2004) Large-scale carbon isotope fractionation in evaporites and the generation of extremely ^{13}C -enriched methane. *Geology*, 32(6), 533–536. <https://doi.org/10.1130/G20323.1>
- Raigemborn, M.S., Cuitiño, J.I., Lizzoli, S., Muñoz, N.A., Bargo, M.S. & Vizcaino, S.F. (2021) Los paleosuelos de la Formación Santa Cruz y el registro climático del Mioceno temprano-medio en Patagonia Austral. Actas XVII Reunión Argentina de Sedimentología y VIII Congreso Latinoamericano de Sedimentología, Paraná Entre Ríos, p. 125.
- Ramos, M.E., Orts, D.L., Calatayud, F., Pazos, P.J., Folguera, A. & Ramos, V.A. (2011) Estructura, Estratigrafía y evolución tectónica de la cuenca de Ñirihuau en las nacientes del río Cushamen, Chubut. *Revista de la Asociación Geológica Argentina*, 68, 210–224.
- Ramos, M.E., Tobal, J.E., Sagripanti, L., Folguera, A., Orts, D.L., Giménez, M. & Ramos, V.A. (2015) The North Patagonian orogenic front and related foreland evolution during the Miocene, analyzed from synorogenic sedimentation and U/Pb dating ($\sim 42^\circ\text{S}$). *Journal of South American Earth Sciences*, 64, 467–485. <https://doi.org/10.1016/j.jsames.2015.08.006>
- Ramos, V.A. (1982) Las ingresiones pacíficas del Terciario en el norte de la Patagonia (Argentina). 3 Congreso Geológico Chileno, pp. 262–288.
- Rapela, C.W., Spalletti, L.A., Merodio, J.C. & Aragón, E. (1988) Temporal evolution and spatial variation of early Tertiary volcanism in the Patagonian Andes (40 S–42 30' S). *Journal of South American Earth Sciences*, 1(1), 75–88. [https://doi.org/10.1016/0895-9811\(88\)90017-X](https://doi.org/10.1016/0895-9811(88)90017-X)
- Reading, H.G. (1996) *Sedimentary environments: processes, facies and stratigraphy*, 3rd edition. Cambridge, MA: Blackwell Science.
- Reading, H.G. & Collinson, J.D. (1996) Clastic coasts. In: Reading, H.G. (Ed.) *Sedimentary environments: processes, facies and stratigraphy*, 3rd edition. Cambridge, MA: Blackwell Science, pp. 154–232.
- Reading, H.G. & Level, B.K. (1996) Controls on sedimentary rock record. In: Reading, H.G. (Ed.) *Sedimentary environments: processes, facies and stratigraphy*, 3rd edition. Cambridge, MA: Blackwell Science, pp. 5–37.
- Richter, D.K., Götze, T., Götze, J. & Neuser, R.D. (2003) Progress in application of cathodoluminescence (CL) in sedimentary petrology. *Mineralogy and Petrology*, 79, 127–166. <https://doi.org/10.1007/s00710-003-0237-4>
- Ricketts, R.D. & Anderson, R.F. (1998) A direct comparison between the historical record of lake level and $\delta 18\text{O}$ signal in carbonate sediments from Lake Turkana, Kenya. *Limnology and Oceanography*, 43(5), 811–822. <https://doi.org/10.4319/lo.1998.43.5.0811>
- Roth, S. (1922) Investigaciones geológicas en la región norte de la Patagonia durante los años 1897 y 1898. *Revista Museo de la Plata*, 26, 393–473.
- Santonja, C., Bechis, F., Suriano, J., Falco, J.I., Encinas, A., Olaizola, E.R., Valencia, V., Litvak, V.D. & Ramos, V.A. (2021) Tectono-stratigraphic evolution of the northeastern sector of the Ñirihuau Basin, North Patagonian Andes, Argentina: insights from sedimentology and geochronology data of the Ñirihuau Formation. *Journal of South American Earth Sciences*, 8th ISAG Special Issue, 111, 103487. <https://doi.org/10.1016/j.jsames.2021.103487>
- Savin, S.M., Douglas, R.G. & Stehli, F.G. (1975) Tertiary marine paleotemperatures. *Geological Society of America Bulletin*, 86(11), 1499–1510. [https://doi.org/10.1130/0016-7606\(1975\)86<1499:TMP>2.0.CO;2](https://doi.org/10.1130/0016-7606(1975)86<1499:TMP>2.0.CO;2)
- Schrag, D.P., Higgins, J.A., Macdonald, F.A. & Johnston, D.T. (2013) Authigenic carbonate and the history of the global carbon cycle. *Science*, 339, 540–543. <https://doi.org/10.1126/science.1229578>
- Scholle, P.A. & Ulmer-Scholle, D.S. (2003) A color guide to the petrography of carbonate rocks: Grains, textures, porosity, diagenesis. *AAPG Memoir*, 77, 461. <https://doi.org/10.1306/M77973>
- Schwalb, A. & Dean, W.E. (2002) Reconstruction of hydrological changes and response to effective moisture variations from north-central USA lake sediments. *Quaternary Science Reviews*, 21(12–13), 1541–1554. [https://doi.org/10.1016/S0277-3791\(01\)00121-4](https://doi.org/10.1016/S0277-3791(01)00121-4)
- Shackleton, N.J. (1987) The carbon isotope record of the Cenozoic: history of organic carbon burial and of oxygen in the ocean and atmosphere. *Geological Society, London, Special Publications*, 26(1), 423–434. <https://doi.org/10.1144/GSL.SP.1987.026.01.27>
- SERNAGEOMIN. (2003) Mapa Geológico de Chile, Versión Digital, Base Geológica escala 1:1.000.000. Publicación Geológica

- Digital, No. 4, CD-ROM, versión 1.0., Servicio Nacional de Geología y Minería.
- Somoza, R. (1998) Updated azca (Farallon)—South America relative motions during the last 40 My: implications for mountain building in the central Andean region. *Journal of South American Earth Sciences*, 11(3), 211–215. [https://doi.org/10.1016/S0895-9811\(98\)00012-1](https://doi.org/10.1016/S0895-9811(98)00012-1)
- Spalletti, L.A. (1981) Facies sedimentarias de la Formación Ñirihuau en la región de San Carlos de Bariloche, provincia de Río Negro. *Revista de la Asociación Geológica Argentina*, 36(3), 288–311.
- Spalletti, L.A. (1983) Paleogeografía de la Formación Ñirihuau y sus equivalentes en la región Occidental de Neuquén, Río Negro y Chubut. *Revista de la Asociación Geológica Argentina*, 38(3–4), 454–468.
- Super, J.R., Thomas, E., Pagani, M., Huber, M., O'Brien, C. & Hull, P.M. (2018) North Atlantic temperature and pCO₂ coupling in the early-middle Miocene. *Geology*, 46(6), 519–522. <https://doi.org/10.1130/G40228.1>
- Swart, P.K. (2015) The geochemistry of carbonate diagenesis: the past, present and future. *Sedimentology*, 62(5), 1233–1304. <https://doi.org/10.1111/sed.12205>
- Swart, P.K., Burns, S.J. & Leder, J.J. (1991) Fractionation of the stable isotopes of oxygen and carbon in carbon dioxide during the reaction of calcite with phosphoric acid as a function of temperature and technique: chemical geology. *Isotope Geoscience Section*, 86(2), 89–96. [https://doi.org/10.1016/0168-9622\(91\)90055-2](https://doi.org/10.1016/0168-9622(91)90055-2)
- Taher, A.G. & Abdel-Motelib, A. (2014) Microbial stabilization of sediments in a recent salina, Lake Aghormi, Siwa Oasis, Egypt. *Facies*, 60, 45–52. <https://doi.org/10.1007/s10347-013-0363-3>
- Talbot, M.R. (1990) A review of the palaeohydrological interpretation of carbon and oxygen isotopic ratios in primary lacustrine carbonates. *Chemical Geology*, 80, 261–279. [https://doi.org/10.1016/0168-9622\(90\)90009-2](https://doi.org/10.1016/0168-9622(90)90009-2)
- Talbot, M.R. & Allen, P.A. (1996) Lakes. In: Reading, H.G. (Ed.) *Sedimentary environments: processes, facies and stratigraphy*, 3rd edition. Cambridge, MA: Blackwell Science, pp. 83–124.
- Teranes, J.N., McKenzie, J.A., Bernasconi, S.M., Lotter, A.F. & Sturm, M. (1999) A study of oxygen isotopic fractionation during bio-induced calcite precipitation in eutrophic Baldeggersee, Switzerland. *Geochimica et Cosmochimica*, 63(13–14), 1981–1999. [https://doi.org/10.1016/S0016-7037\(99\)00049-6](https://doi.org/10.1016/S0016-7037(99)00049-6)
- Tucker, M.E. & Wright, V.P. (1990) *Carbonate sedimentology*. Oxford: Blackwell Scientific Publications.
- Tucker, M. & Wright, P. (2002) *Carbonate sedimentology*. United Kingdom: Blackwell Science, p. 482.
- Turner, J.V., Fritz, P., Karrow, P.F. & Warner, B.G. (1983) Isotopic and geochemical compositions of marl lake waters and implications for radiocarbon dating of marl lake sediments. *Canadian Journal of Earth Sciences*, 20(4), 599–615. <https://doi.org/10.1139/e83-056>
- Uliana, M.A. & Biddle, K.T. (1988) Mesozoic–Cenozoic paleogeographic and geodynamic evolution of southern South America. *Revista Brasileira de Geociencias*, 18, 172–190.
- Valero-Garcés, B.L., Delgado-Huertas, A., Ratto, N. & Navas, A. (1999) Large ¹³C enrichment in primary carbonates from Andean Altiplano lakes, northwest Argentina. *Earth and Planetary Science Letters*, 171(2), 253–266. [https://doi.org/10.1016/S0012-821X\(99\)00150-8](https://doi.org/10.1016/S0012-821X(99)00150-8)
- Valero-Garcés, B.L., Gierlowski-Kordesch, E.H. & Bragonier, W.A. (1997) Pennsylvanian continental cyclothem development: no evidence of direct climatic control in the Upper Freeport Formation (Allegheny Group) of Pennsylvania (northern Appalachian Basin). *Sedimentary Geology*, 109(3–4), 305–319. [https://doi.org/10.1016/S0037-0738\(96\)00071-1](https://doi.org/10.1016/S0037-0738(96)00071-1)
- Vázquez-Urbez, M., Arenas, C., Pardo, G. & Pérez-Rivarés, J. (2013) The effect of drainage reorganization and climate on the sedimentologic evolution of intermontane lake systems: the final fill stage of the Tertiary Ebro Basin (Spain). *Journal of Sedimentary Research*, 83(8), 562–590. <https://doi.org/10.2110/jsr.2013.47>
- Wright, J.D., Miller, K.G. & Fairbanks, R.G. (1992) Early and Middle Miocene stable isotopes: implications for deep-water circulation and climate. *Paleoceanography and Paleoclimatology*, 7(3), 357–389. <https://doi.org/10.1029/92PA00760>
- Wright, V.P. (1992) A revised classification of limestones. *Sedimentary Geology*, 76(3–4), 177–185. [https://doi.org/10.1016/0037-0738\(92\)90082-3](https://doi.org/10.1016/0037-0738(92)90082-3)
- Yansa, C.H., Dean, W.E. & Murphy, E.C. (2007) Late Quaternary paleoenvironments of an ephemeral wetland in North Dakota, USA: relative interactions of ground-water hydrology and climate change. *Journal of Paleolimnology*, 38, 441–457. <https://doi.org/10.1007/s10933-006-9079-5>
- You, Y., Huber, M., Müller, R.D., Poulsen, C.J. & Ribbe, J. (2009) Simulation of the Middle Miocene climate optimum. *Geophysical Research Letters*, 36(4), L04702. <https://doi.org/10.1029/2008GL036571>
- Zachos, J.C., Dickens, G.R. & Zeebe, R.E. (2008) An early Cenozoic perspective on greenhouse warming and carbon-cycle dynamics. *Nature*, 451(7176), 279–283. <https://doi.org/10.1038/nature06588>
- Zachos, J., Pagani, M., Sloan, L., Thomas, E. & Billups, K. (2001) Trends, rhythms, and aberrations in global climate 65 Ma to present. *Science*, 292(5517), 686–693. <https://doi.org/10.1126/science.1059412>

How to cite this article: Santonja, C., Benavente, C.A., Suriano, J., Heredia, A.M., Fortunatti, N., Rainoldi, A.L. et al. (2025) The Miocene lacustrine carbonate factory of the Ñirihuau Formation, Ñirihuau Basin, North Patagonian Andes, Argentina. *The Depositional Record*, 11, 147–181. Available from: <https://doi.org/10.1002/dep2.291>